BMC Complementary Medicine and Therapies

RESEARCH

Open Access

Bioprospection of indigenous herbal formulations for diabetes care: in vitro, network pharmacology, and molecular dynamics studies

Oluwafemi Adeleke Ojo[1,2*], Akingbolabo Daniel Ogunlakin[2], Omolola Adenike Ajayi-Odoko[3], Gideon Ampoma Gyebi[4], Damilare IyinKristi Ayokunle[5], Adesoji Alani Olanrewaju[6], Oluwatobi Deborah Agbeye[2], Emmanuel Tope Ogunwale[7] and Oluyomi Stephen Adeyemi[2]

Abstract

Background Herbal formulations have garnered significant interest from researchers for their potential antidiabetic effects. However, scientific validation of their efficacy and understanding of their mechanisms of action have limited their use in modern medicine. Therefore, we investigated crude formulations consisting of *Beta* vulgaris leaves, *Persea americana* seeds, *Beta vulgaris* roots and *Syzygium aromaticum* for the management of type 2 diabetes mellitus (T2DM) by combining network pharmacology with experimental verification.

Methods We screened 11 active ingredients and 3238 corresponding targets from biological databases. Additionally, the stability of the top-ranked poses and positive compounds linked to DPP-IV, α-amylase, and α-glucosidase were evaluated via molecular dynamics.

Results Herbal formulations Formulations A and B exhibited notable inhibitory activity against the α-amylase enzyme, with IC_{50} values of 113.325. ± 6.627 and 170.704 ± 5.658 µg/mL, respectively, compared with that of acarbose (IC_{50} = 27.704 ± 0.270 µg/mL). Notably, Formulation B (IC_{50} = 15.035 ± 4.582 µg/mL) exhibited greater inhibitory activity than both Formulation A (IC_{50} = 271.835 ± 5.601 µg/mL) and the standard acarbose (IC_{50} = 17.389 ± 0.436 µg/mL). In addition, both Forms A (IC_{50} = 150.953 ± 23.127 µg/mL) and B (IC_{50} = 194.706 ± 37.776 µg/mL) showed notable inhibitory activity against DPP-IV compared with the standard evogliptin (IC_{50} = 86.534 ± 6.043 µg/mL). Furthermore, neither crude formulation exhibited cellular toxicity in human foreskin fibroblasts, with IC_{50} values for formulation A (1949 µg/mL) being lower than those for formulation B (7580 µg/mL). On the basis of our findings, the main active components, namely, quercetrin, rutin, and myricetin, exhibit strong binding affinities and stability for DPP-IV, α-amylase, and α-glucosidase. According to the results of the GO and KEGG analyses, the use of crude formulations to treat T2D may affect various pathways, including the EGFR and PI3K/Akt pathways.

*Correspondence:
Oluwafemi Adeleke Ojo
oluwafemiadeleke08@gmail.com; olaojo@utu.fi

Full list of author information is available at the end of the article

© The Author(s) 2025. **Open Access** This article is licensed under a Creative Commons Attribution-NonCommercial-NoDerivatives 4.0 International License, which permits any non-commercial use, sharing, distribution and reproduction in any medium or format, as long as you give appropriate credit to the original author(s) and the source, provide a link to the Creative Commons licence, and indicate if you modified the licensed material. You do not have permission under this licence to share adapted material derived from this article or parts of it. The images or other third party material in this article are included in the article's Creative Commons licence, unless indicated otherwise in a credit line to the material. If material is not included in the article's Creative Commons licence and your intended use is not permitted by statutory regulation or exceeds the permitted use, you will need to obtain permission directly from the copyright holder. To view a copy of this licence, visit http://creativecommons.org/licenses/by-nc-nd/4.0/.

Conclusion These results provide a scientific and experimental foundation for the use of these particular plants for the treatment of T2D.

Keywords Computational modeling, Drug discovery and development, Herbal drug formulation, Metabolic diseases, Network pharmacology

Introduction

Carbohydrate and lipid metabolism are pivotal for energy homeostasis and are tightly controlled in healthy individuals. However, as people age, the prevalence of lipid and glucose metabolic disorders (LGMDs) increases, resulting in health issues such as dyslipidemia, obesity, atherosclerosis, fatty liver, and type 2 diabetes mellitus (T2DM) [1, 2]. Among these diseases, type 2 diabetes mellitus (T2DM) has attracted the attention of researchers because of its status as a global pandemic [3]. T2DM is characterized by persistent hyperglycemia caused by both insulin resistance and inadequate insulin production and secretion [4]. As T2DM progresses, it can have a substantial effect on multiple organs, resulting in complicated implications such as neuropathy, renal disease, retinopathy, and macrovascular problems [5]. While a number of oral anti-type 2 diabetes drugs, such as sitagliptin, metformin, and sulfonylureas, have exhibited promising effects in treating T2DM, these drugs mainly target one pathway, which frequently has negative side effects [6]. Therefore, exploring similar and alternative medical approaches for efficient T2DM management is essential. African traditional medicine (ACM) often involves mixtures of medicinal plant species and minerals, which can lead to synergistic effects by functioning at various levels on many targets and pathways within the disease network [7, 8]. This method allows research into the synergistic effects of ACM by closing the gap between modern and traditional medicine. By leveraging multiple components and targets, ACM aims to achieve better therapeutic efficacy while minimizing side effects [8].

Owing to their accessibility, cost-effectiveness, and fewer side effects, natural medicines continue to be widely used by the general public even in the modern period, when synthetic medications dominate the therapeutic market. The bioactive substances found in plant extracts have been extensively investigated. The phytoconstituents of medicinal plants, including phenolics, flavonoids, terpenoids, and tannins, play crucial roles in managing diabetes (DM). By acting on cell receptors or biological targets, herbal products, prescription medications, and biochemical agents have synergistic effects that improve therapeutic results [9]. Synergy occurs when molecules work together to produce a combined effect that exceeds the sum of their separate effects. In a synergistic effect, multiple agents target similar biological targets or receptors, leading to enhanced therapeutic outcomes due to positive interactions [10]. Conversely, additive effects result from two phytoconstituents acting together, with their effects simply adding up [11]. In our study, we collected four medicinal plants from various areas in Nigeria. These plants were mixed in different ratios to create two distinct herbal formulations. Both additive and synergistic effects are thought to contribute to the hypoglycemic activity of these combination formulations. The therapeutic plants selected included *Beta vulgaris* leaves, *Persea americana* seeds, *Beta vulgaris* roots and *Syzygium aromaticum*.

Beetroot (*Beta vulgaris* L.) is widely recognized as a valuable food source that offers significant nutritional and health benefits. Its medicinal properties are largely attributed to its high concentration of bioactive compounds, particularly phenolic substances such as flavonoids and phenolic acids, and notably, it stands out as the most abundant natural source of betalains. These diverse phytochemicals are responsible for the broad spectrum of biological activities of beetroot, including antioxidant, anti-inflammatory, antihypertensive, hepatoprotective, hypoglycemic, and potential antidepressant effects [12–14]. Historically, the high levels of these bioactive secondary metabolites have led to the use of beetroot in traditional medicine, and modern research continues to explore its extracts for their beneficial properties, including antibacterial actions. The variety of bioactive chemicals found in beetroot accounts for its wide range of activity [12].

P. americana, commonly known as avocado, is a valuable fruit with significant pharmacological potential. Avocado seeds have been studied extensively and exhibit various health-promoting activities. These effects include antioxidant, anti-inflammatory, antihypertensive, hepatoprotective, and hypolipidemic effects. Additionally, avocado seeds may aid in managing conditions such as hypertension, inflammatory disorders, and diabetes [15]. They also possess insecticidal, fungicidal, and antimicrobial properties [16, 17]. The rich diversity of bioactive compounds in avocado contributes to its multifaceted therapeutic benefits.

S. aromaticum, widely recognized as a clove, is a known traditional spice with a rich history of use in food preservation. In addition to its culinary applications, clove possesses various pharmacological activities due to its abundant phytochemicals [18]. Notable compounds found in clove include eugenol, eugenyl acetate, and β-caryophyllene. Pharmacological research has shown that clove has antimicrobial properties against bacteria,

hepatitis C viruses, *Plasmodium*, *Babesia*, and *Herpes simplex*. Eugenol, a major component of clove oil, has analgesic, antioxidant, anticancer, antiseptic, and anti-inflammatory properties [19]. Despite advancements in medicinal plant research, the specific components and associated targets of crude formulations for T2DM remain unclear and warrant further investigation.

The convergence of bioinformatics, artificial intelligence, and methods such as dynamic simulation, molecular docking, and network pharmacology has indeed emerged as an interdisciplinary approach to comprehensively study African traditional medicine (ATM). Researchers are increasingly integrating computational approaches, clinical trials, and experimental methods to enhance our understanding of traditional complementary medicine (TCM) processes. This comprehensive approach allows for a deeper exploration of the mechanisms underlying traditional medicine practices and their potential applications in modern health care [20, 21]. Although herbal plants are extensively utilized by diverse indigenous and ethnic communities worldwide, only limited scientific studies exist to validate their efficacy. The aim of this study was to verify the effectiveness of a few selected plant remedies by scientific and experimental means, taking into account the references provided and utilizing these plants in complementary and alternative therapies. This work integrated network pharmacology, molecular dynamics simulation docking, and experimental research to determine the active constituents, putative targets, and underlying processes of the anti-T2DM effects of crude drug formulations.

Methods

Chemicals

For chromatographic analysis, chromatographic-grade methanol was obtained from J.T. Baker (USA), phosphoric acid (H3PO4) was obtained from EM Science (USA), and tetrahydrofuran was obtained from EM Science (USA). A suite of standard compounds, including gallic acid, ferulic acid, kaempferol, quercetrin, caffeic acid, myricetin, rutin, methyl gallate, syringic acid, and p-coumaric acid, were procured from Sigma Aldrich. Human foreskin fibroblasts (HFFs) were routinely maintained in Dulbecco's modified Eagle's medium (DMEM; Sigma, Tokyo, Japan) supplemented with 5% (v/v) fetal calf serum (FCS; Gibco, Invitrogen, UK) and 1% penicillin–streptomycin (Biowhittaker, UK) at 37 °C in a 5% CO2 atmosphere.

Table 1 List of chosen medicinal plants

Scientific name	Family	Local name	English name	Part Used	Crude voucher No
Beta vulagris	Amaranthaceae	Ewe beet	Beet green	Leaf	FHI 114,105
Persea americana	Lauraceae	Ube-beke	Avocado	Seed	FHI 113,162
Beta vulgaris	Amaranthaceae	Gbẹ̀ri beet	Red beet	Root	FHI 114,105
Syzygium aromaticum	Myrtaceae	Kanafuru	Clove	Flower bud	FHI 114,106

Plant sample collection and identification

In October 2020, selected medicinal plant materials, specifically *B. vulgaris* leaves and roots, *P. americana* seeds, and *S. aromaticum* buds (as detailed in Table 1), were procured from an herbal vendor in Ado-Ekiti, Nigeria (7.6124° N, 5.2371° E). Taxonomic identification and herbarium preparation were conducted by Mr. Odewo at the Forestry Research Institute of Nigeria (FRIN), Ibadan. Voucher samples for each plant were subsequently archived at the FRIN herbarium under accession codes FH1 114,105 (*B. vulgaris* leaves and roots), FHI113162 (*P. americana* seeds), and FHI 114,106 (*S. aromaticum* buds). Following collection, the plant samples underwent immediate processing: they were rinsed thoroughly, sectioned into smaller pieces, and initially air-dried in a shaded area. Final drying to a consistent weight was achieved via the use of an air oven set at 40 °C, after which the dried materials were pulverized into a fine powder and sieved.

Flavonoid-rich extraction and crude drug formulations

To obtain flavonoid-rich extracts, powdered samples (50 g each) of *B. vulgaris* leaves and roots, *P. americana* seeds, and *S. aromaticum* buds were initially subjected to 72 h of maceration in 80% methanol. The resulting crude methanolic extract (20 g) then underwent acid hydrolysis using 10% H_2SO_4 (200 mL) at 100 °C for 30 min, followed by cooling on ice to precipitate the flavonoid aglycones. These aglycones were subsequently dissolved in warm 95% ethanol (50 mL) and filtered, and the volume was adjusted to 100 mL with 95% ethanol. After concentrating via rotary evaporation, the flavonoids were precipitated from the filtrate via concentrated NH_4OH. The precipitate was allowed to settle and then washed with diluted NH_4OH to yield the final flavonoid extracts [22]. Two distinct formulations (A and B, detailed in Table S1) were then prepared by combining these crude flavonoid-rich extracts at specific ratios. The flavonoid extracts were dissolved in DMSO (1:5 w/v) and subjected to a single 24 h maceration. This formulation strategy was based on guidance from a traditional medicine practitioner in Iwo, Nigeria. The obtained crude formulations were utilized for subsequent preclinical investigations.

High-performance liquid chromatography (HPLC) analysis of crude formulations A and B

Chromatographic separation was performed via an Agilent Technologies 1100-series HPLC system equipped with a quaternary pump and a UV-Diode Array Detector (DAD) (Agilent, San Jose, CA, USA). A Zorbax Eclipse Plus C18 column (250 mm × 4.6 mm, 5 µm particle size; Agilent Technologies, USA) was used for the analysis. The mobile phase consisted of a gradient mixture of water (containing 1% H3PO4), methanol (MeOH), and tetrahydrofuran (THF), which was delivered at a flow rate of 1.5 mL/min. For each analysis, a 20 µL sample volume was injected. The chromatographic run involved a 10 min mobile phase purge and a 10 min column equilibration period, followed by a 35 min sample analysis time. Spectral data were acquired at a detection wavelength of 220 nm, following a previously established methodology [23].

In vitro antidiabetic activities

α-Amylase inhibitory properties

In this investigation, we evaluated the α-amylase inhibitory activity of crude drug formulations A and B via the methodology outlined elsewhere [24]. First, we made an enzyme mixture in ice-cold PBS (pH 6.7) with 20 mM and 6.7 mM NaCl. The concentration of this solution was 5 units/mL. After that, we mixed the inhibitors (acarbose or crude drug formulations A and B) at different doses with 250 µL of the enzyme, leaving out a blank sample. The reaction was developed by heating the mixture in a 100 °C water bath for 10 min, after which the absorbance was measured at 540 nm.

Inhibitory properties of α-glucosidase

Using a method described by [25], we evaluated the effects of the formulations on intestinal α-glucosidase activity. This method calculates the amount of glucose generated during the hydrolysis of sucrose. A positive control (acarbose), control samples (distilled water), or crude drug formulations A and B at different concentrations were added to the combination. At 400 nm, the absorbance of the resulting solution was measured.

Activity of dipeptidyl peptidase IV (DPP-IV)

In this work, we used 96-well ELISA plates to assess the DPP-IV inhibitory properties of the formulations. Evogliptin was used as a standard inhibitor. Briefly, we added 100 µL of DPP-IV enzyme, 30 µL of Tris-HCl buffer solution, and 100 µL of different doses (from 15.625 to 1000 µg/mL) of standard or crude drug formulations A and B to each well. Furthermore, 50 µL of gly-pro-p nitroanilide was added as the substrate. Following a 30 min incubation period at 37 °C, the absorbance of the reaction mixture was quantified at 405 nm via a microplate reader [26]. The percentage inhibition was subsequently determined via the following formula:

$$\%\, Inhibition = \frac{DPP-IV\ activity\ (with\ fraction)}{DPP-IV\ activity\ (without\ fraction)} \times 100$$

Cytotoxicity in mammalian cells

Cytotoxicity was evaluated in mammalian cells via a previously reported method [27]. For the experimental assays, HFFs were seeded at a density of 1×10^4 cells/well into 96-well plates. Following 72 h of preincubation, the cells were exposed to the test compounds (0–1000 µg/mL) for an additional 72 h under standard culture conditions. The control groups consisted of medium-only wells and cells cultured with medium devoid of test compounds; staurosporine was employed as a reference toxicant. The cell viability was subsequently quantified, all the treatments were performed in triplicate, and the entire experiment was independently replicated twice.

Integrated network Pharmacology and molecular dynamics

Seeking putative target genes for bioactive compounds

SMILES (Simplified Molecular Input Line Entry System) notations for bioactive compounds identified by HPLC from formulations A and B were retrieved from the PubChem database (accessed July 12, 2024) [28]. The potential protein targets of these HPLC-identified compounds in *H. sapiens* were subsequently predicted via the SwissTarget prediction web server (accessed July 14, 2024) [29, 30]. On July 12, 2024, further targets were obtained from PharmMapper (http://www.lilabecust.cn/pharmmapper/). Only targets with a probability of ≥ 0.1 were considered after we filtered the results in the SwissTarget prediction platform using the species *Homo sapiens* [31].

Constructing the target database for T2DM

By scanning the DisGeNet database (https://www.disgenet.org/, retrieved on 14 July 2024) [32], MalaCards (accessed on July 14, 2024, from https://www.malacards.org/) [33] and the Online Mendelian Inheritance in Man (OMIM) [34], which was accessed on July 14, 2024, from https://www.omim.org, T2DM-related genes were identified. Targets with a score of ≥ 0.1 were considered for inclusion [31].

Identifying bioactive compound targets for treating T2DM

The overlapping targets were extracted from the putative targets of the bioactive substances and all the T2DM-related targets [22]. Networks were further constructed using the overlapping genes.

Constructing the interaction network of bioactive compounds from flavonoid formulations A and B with T2DM targets

A protein–protein interaction (PPI) network for *Homo sapiens* was created via the STRING database (accessed July 12, 2024) [29], with interactions filtered to a high confidence score (> 0.9) [35]. This network, where nodes represent the target genes (proteins) and edges depict the interactions between them, was visualized and further analyzed. Key hub genes and significant nodes within this network were identified via the CytoHubba plugin [36] in Cytoscape, a tool designed for exploring and analyzing biomolecular interaction networks.

Pathway analysis and functional enrichment

Enrichment analyses, encompassing both KEGG pathway and Gene Ontology (GO) terms, were carried out on the set of intersecting genes via the ShinyGO v0.77 tool (accessed July 12, 2024) [37]. The top 10 significantly enriched terms, determined by a p value < 0.05 and a false discovery rate (FDR) < 0.05, are presented.

Molecular Docking of bioactive compounds with target proteins

Target protein Preparation

The three-dimensional (3D) coordinates for two target proteins relevant to T2DM were obtained from the Protein Data Bank. These structures include human α-amylase bound to acarbose (PDB ID: 1B2Y) [38] and α-glucosidase bound to acarbose (PDB ID: 3TOP) [39] and DPP4 in complex with vildagliptin (PDBID: 6B1E) [40], Akt1 (PDBID: 6CCY), STAT3 (PDBID: 4ZIA), P53 (PDBID: 2°CJ), and TNF-alpha (PDBID: 2AZ5) [41].

Ligand preparation

Structural data (SDF files) for the HPLC-identified phytocompounds from formulations A and B, along with reference inhibitors acarbose and vildagliptin, were sourced from the PubChem database. These structures were subsequently converted to the PDB file format via Open Babel [42].

Validation of the molecular Docking analysis

The docking protocol was validated by redocking the cocrystallized ligand (acarbose) into the binding sites of its respective proteins. Specifically, the experimentally observed pose of acarbose (extracted from the crystal structure) was compared to its computationally predicted docked pose, which achieved the lowest binding energy. This comparison involved superimposing the two poses, and the root mean square deviation (RMSD) between them was calculated via Discovery Studio Visualizer (BIOVIA, 2020). The successful reproduction of the crystallographic pose confirmed the suitability of the docking methodology for evaluating HPLC-identified bioactive compounds.

Molecular Docking of phytochemicals with targeted active sites

The reference inhibitors and the bioactive compounds identified via HPLC were subjected to an active site target molecular docking process via AutoDock Vina combined with Python prescription-PyRx version 0.8 at the binding sites of the three target proteins [41, 43] (Table S2).

Molecular dynamics simulations

Molecular dynamics (MD) simulations (100 ns) were performed on complexes formed by the top two bioactive compounds with 1B2Y and TNF-alpha via GROMACS 2019.2 with the GROMOS96 43a1 force field [44–46]. Protein and ligand topologies were generated via Charmm-GUI [47, 48]. The system setup, including solvation, physiological conditions, periodic boundaries, minimization, and NPT equilibration, followed our previously established protocols [49–51]. The simulations were maintained at 310 K and 1 atm via a Parrinello–Rahman barostat and velocity rescaling, with a 2-fs timestep and a leap-frog integrator. Trajectories (1000 frames, 0.1 ns/snapshot) were analyzed for parameters such as RMSD, RMSF, SASA, ROG, and H-bond interactions.

Binding affinity assessment by MM-GBSA

Binding free energies for the top two docked bioactive compounds complexed with 1B2Y and TNF-alpha were calculated via the Molecular Mechanics Generalized Born Surface Area (MM-GBSA) method implemented with gmx_MMPBSA software, which also facilitated decomposition analysis [22, 52]. The specific MM-GBSA parameters and procedures employed were consistent with our previously published work [50, 51, 53].

Data analysis

The data were analyzed via one-way analysis of variance (ANOVA), and the results are expressed as the means ± standard deviations (SDs) from three independent experiments ($n = 3$). *Post hoc* comparisons were subsequently performed via Tukey's test followed by Dunnett's multiple range test. The significance level was set at $p < 0.05$.

Results

HPLC–DAD chromatogram

Analysis of the crude formulations by HPLC-DAD revealed distinct profiles of bioactive flavonoids. Formulation A was found to contain six such compounds: syringic acid, rutin, gallic acid, caffeic acid, kaempferol, and

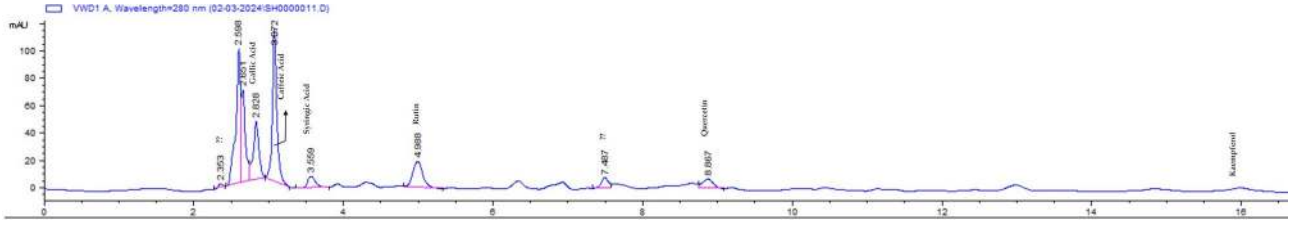

Fig. 1 Chromatogram of crude formulation A

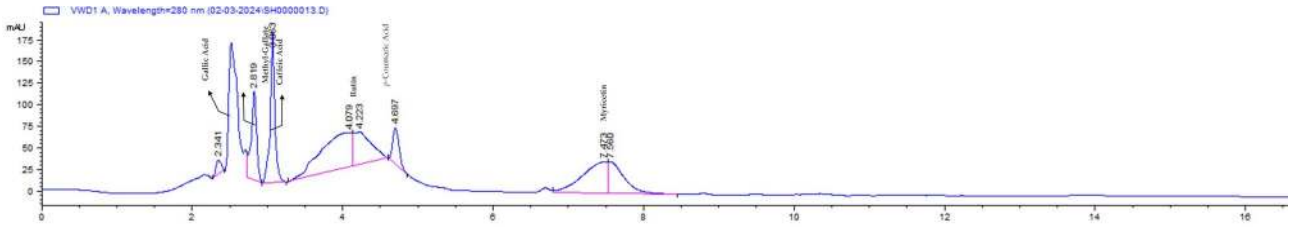

Fig. 2 Chromatogram of crude formulation B

quercetrin. Formulation B yielded seven bioactive flavonoids: caffeic acid, quercetrin, p-coumaric acid, myricetin, rutin, gallic acid, and methyl gallate (as detailed in Table 4 and illustrated in Figs. 1 and 2). Further characterization of these identified compounds, including their respective retention times, molecular formulae, and chemical structures, is provided in Table 2.

α-Amylase and α-glucosidase inhibitory activities

The standard acarbose and crude drug formulations A and B strongly suppressed α-amylase activity in a concentration-dependent manner (Fig. 3a). Compared with crude formulation B, crude formulation A exhibited superior ($p < 0.0001$) α-amylase inhibitory activity, with an IC_{50} of 113.325 ± 6.627 µg/mL and an IC_{50} of 170.585 ± 5.658 µg/mL. In contrast, the standard drug acarbose had better inhibitory effects than did crude formulations A and B, with an IC_{50} of 27.104 ± 0.270 µg/mL (Fig. 3b).

Compared with those of the reference formulation (acarbose), the α-glucosidase inhibitory properties of formulations A and B increased in a dose-dependent manner (Fig. 4A). Furthermore, crude drug formulation B had better inhibitory activity (IC_{50} = 15.035 ± 4.582 µg/mL) than did standard acarbose (IC_{50} = 17.389 ± 0.436 µg/mL) and crude drug formulation A (IC_{50} = 271.839 ± 5.601 µg/mL).

DPP-IV inhibitory activity of the crude drug formulations

Figure 5 shows the DPP-IV inhibitory activity of crude drug formulations A and B. Crude drug formulations A and B demonstrated concentration-dependent inhibition of DPP-IV, with formulation A exhibiting a lower IC_{50} value of 150.95 µg/mL than B (IC_{50} = 194.71 µg/mL) (Fig. 5b). Nevertheless, compared with the standard DPP-IV inhibitor evogliptin (IC_{50} = 86.534 ± 6.043 µg/mL), the DPP-IV inhibitory ability of crude drug formulations A (IC_{50} = 150.953 ± 23.127 µg/mL) and B (IC_{50} = 194.706 ± 37.776 µg/mL) was less effective. However, crude drug formulation A had better DPP-IV inhibitory activity than formulation B.

Cytotoxicity studies

First, we administered forms A and B at several concentrations (ranging from 0 to 1000 µg/mL) to growing HFFs and evaluated their cytotoxicity (Fig. 6). Both crude formulations A and B moderately reduced cell viability in vitro at increasing concentrations, with IC_{50} values for formulation A (1949 µg/mL) being lower than those for formulation B (7580 µg/mL). Both formulations demonstrated biological safety, with no discernible cytotoxicity to HFF cells at the indicated doses after 72 h (Fig. 6A). Our screening assay was validated by the fact that the reference drug (staurosporine), which was used as a positive control, strongly decreased cell viability (Fig. 6B).

Identification of bioactive compounds and database resources for therapeutic targets in T2DM

A comprehensive list of 3238 unique genes linked to T2DM was compiled by integrating data from the MalaCards, DisGeNet, and Online Mendelian Inheritance in Man (OMIM) databases, following duplicate removal. Separately, target prediction for a panel of bioactive compounds yielded 188 potential protein targets. The intersection between these T2DM-associated genes and the predicted compound targets was then determined via a Venn diagram. A group of 119 putative anti-type 2 diabetes mellitus genes were chosen and deemed noteworthy targets (Fig. 7).

Table 2 Bioactive principles identified in crude drug formulations, including retention times, metabolic classes and molecular formulae

Compounds							
Form A	Retention time	Metabolite subclasses	Form B	Retention time	Metabolite subclasses	Structure	Molecular Formulae
			Myricetin	7.560	Flavonol	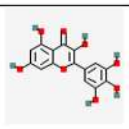	$C_{15}H_{10}O_8$
			p-coumaric acid	4.697	Hydroxycinnamic acid	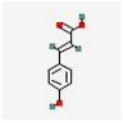	$C_9H_8O_3$
Gallic acid	2.828	Phenolic acid	Gallic acid	2.341	Phenolic acid		$C_7H_6O_5$
Caffeic acid	3.072	Hydroxycinnamic acid	Caffeic acid	3.063	Hydroxycinnamic acid	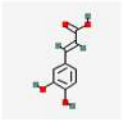	$C_9H_8O_4$
Quercetrin	8.867	Flavonol	Quercetrin	19.536	Flavonol	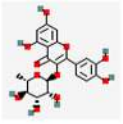	$C_{21}H_{20}O_{11}$
			Methyl gallate	2.819	Galloyl esters	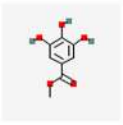	$C_8H_8O_5$
Rutin	4.988	Glycoside flavonol	Rutin	4.079	Glycoside flavonol	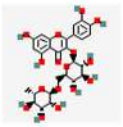	$C_{27}H_{30}O_{16}$
Syringic acid	3.559	Phenolic acid				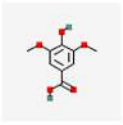	$C_9H_{10}O_5$
Kaempferol	2.353	Tetrahydroxyflavone				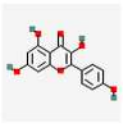	$C_{15}H_{10}O_6$

Target PPI network analysis

Analysis of the PPI network for the overlapping genes revealed 118 nodes and 1238 edges, an average node degree of 21, and a local clustering coefficient of 0.56 (compared with a predicted 524 edges; see Figure S1, Supplementary data). The top 20 targets were subsequently identified by filtering for genes with scores above the median value across all network metrics (Fig. 8). The top 20 targets that were drawn from the overlapping genes of the compound targets and T2D targets

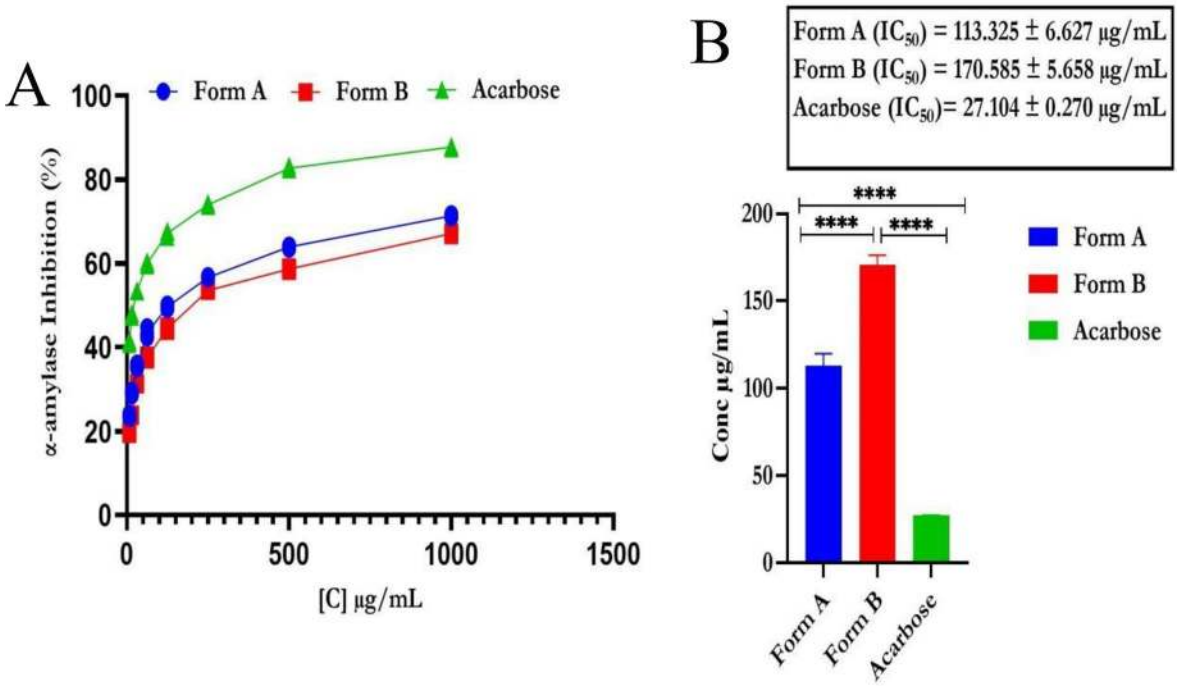

Fig. 3 Alpha-amylase inhibitory activity of formulations A and B: (**a**) Dose–response inhibition; (**b**) calculated IC50 values. **Legends**: Data represent the mean ± SD ($n = 3$). T tests indicated $p < 0.0001$. Acarbose served as the standard drug

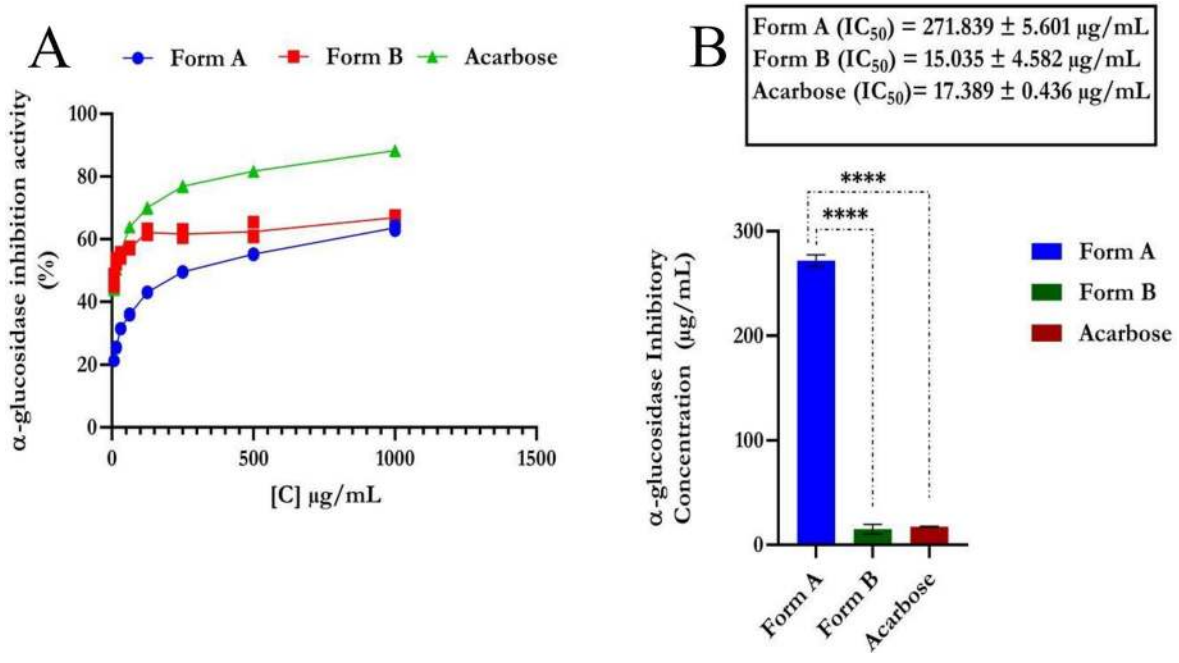

Fig. 4 Alpha-glucosidase inhibitory activity of formulations A and B: (**a**) Dose–response inhibition; (**b**) calculated IC50 values. **Legends**: Data represent the mean ± SD ($n = 3$). T tests indicated $p < 0.0001$. Acarbose served as the standard drug

were mainly inflammatory targets, including TNF, TP53, AKT1, and STAT3, which are not solely implicated in diabetes alone but are major hallmarks of diabetes complications. These targets were further studied via molecular docking and molecular dynamics (Table S3). The constructed network was subsequently imported into Cytoscape software (version 3.8.2) for detailed investigation of significant subnetworks. Cluster analysis within the network was performed utilizing proximity and degree metrics, with scores derived from the CytoHubba

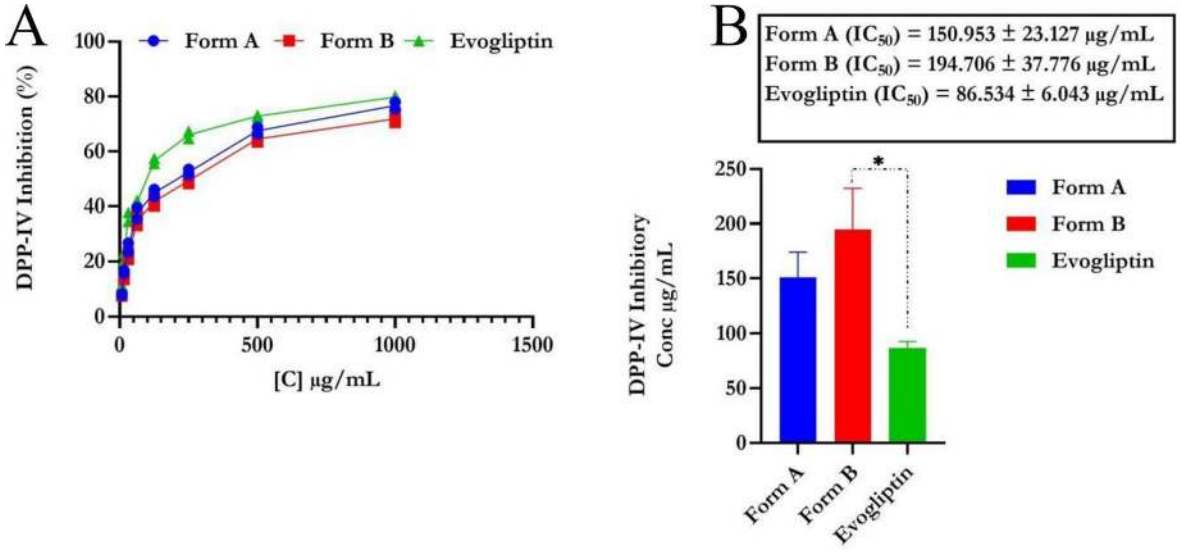

Fig. 5 Dipeptidyl peptidase-4 inhibitory activity of formulations A and B: (**a**) dose–response inhibition; (**b**) calculated IC50 values. **Legends**: Data represent the mean ± SD ($n = 3$). T tests indicated $p < 0.0001$. Acarbose served as the standard drug

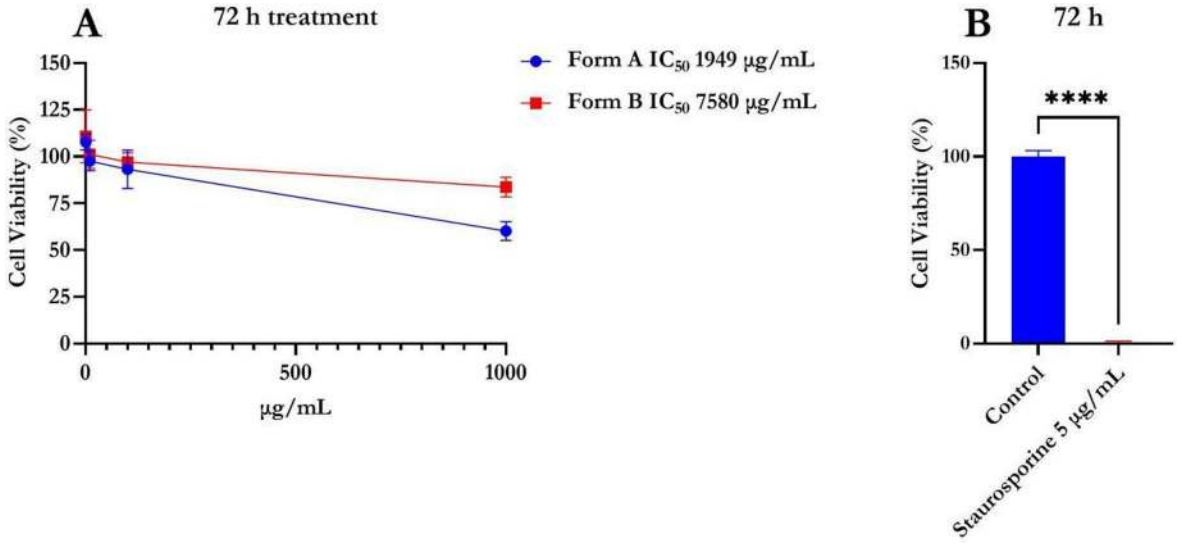

Fig. 6 Effects of crude drug formulations on cell viability following 72 h of treatment. The cytotoxicity of the (**A**) crude formulations A and B is displayed in the dose–response curve. (**B**) Viability of the reference compound staurosporine. Following a 72 h incubation period, the test molecules were applied to the host monolayers at various doses, and the IC_{50} values for the crude drug formulations and cell viability were ascertained. Staurosporine was included as a reference toxicant to validate the assay. The data are presented as the means ± standard deviations (SDs). We performed the experiment in triplicate and repeated it two times independently

and CytoNca plugins. Finally, the top 20 target genes were identified by selecting those whose associated analytical values surpassed the median score across all entities.

Functional enrichment analysis of shared targets

The top 20 enriched genes from the 119 overlapping targets were identified via Gene Ontology (GO) analysis. Subsequent biological process (BP) enrichment (Fig. 9A) suggested that the bioactive compounds predominantly influence cellular responses and reactions to nitrogenous, oxygen-containing, and organonitrogen compounds. With respect to cellular processes, the most enriched terms were the following: spanning components of the plasma membrane, caveolae, membrane rafts, and membrane microdomains (Fig. 9B). The enriched molecular functions (MFs) included identical protein binding, enzyme binding, protein/threonine/serine/tyrosine kinase activity, catalytic activity acting on protein, and carbohydrate derivative binding (Fig. 9C). KEGG pathway enrichment analysis revealed that the bioactive compounds were associated with cancers, EGFR tyrosine

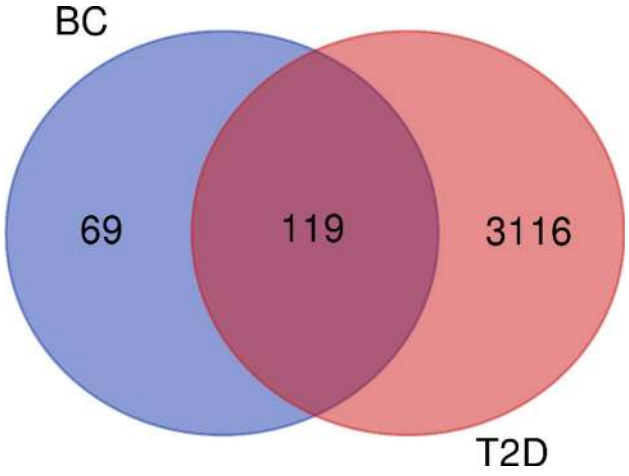

Fig. 7 Overlap between T2DM-related genes and targets of bioactive compounds in formulations A and B, visualized by a Venn diagram. Among the T2DM and bioactive compound targets, 119 shared genes were identified. (BC: bioactive compound target

kinase inhibitor resistance, lipid and atherosclerosis, endocrine resistance, and the P13k-Akt signaling pathway (Fig. 9D).

Molecular docking of bioactive compounds with key targets

To ensure the reliability of the docking procedure for evaluating bioactive compounds against T2DM target proteins, the protocol was first validated. This involved redocking the cocrystallized ligand, acarbose, into its respective protein structure. The computationally predicted pose of acarbose yielding the lowest binding energy was then superimposed onto its experimentally determined (cocrystallized) conformation, resulting in an RMSD of 0.2232 Å (Fig. 10), confirming the accuracy of the docking methodology. Following validation, the binding energies of the identified bioactive compounds against three T2DM target proteins were determined (Fig. 11), and the two leading compounds for each target were selected on the basis of these energies. For reference, acarbose exhibited binding energies of -12.3 kcal/mol with 1B2Y and – 11.1 kcal/mol with 3TOP, whereas vildagliptin had a binding energy of -6.7 kcal/mol with

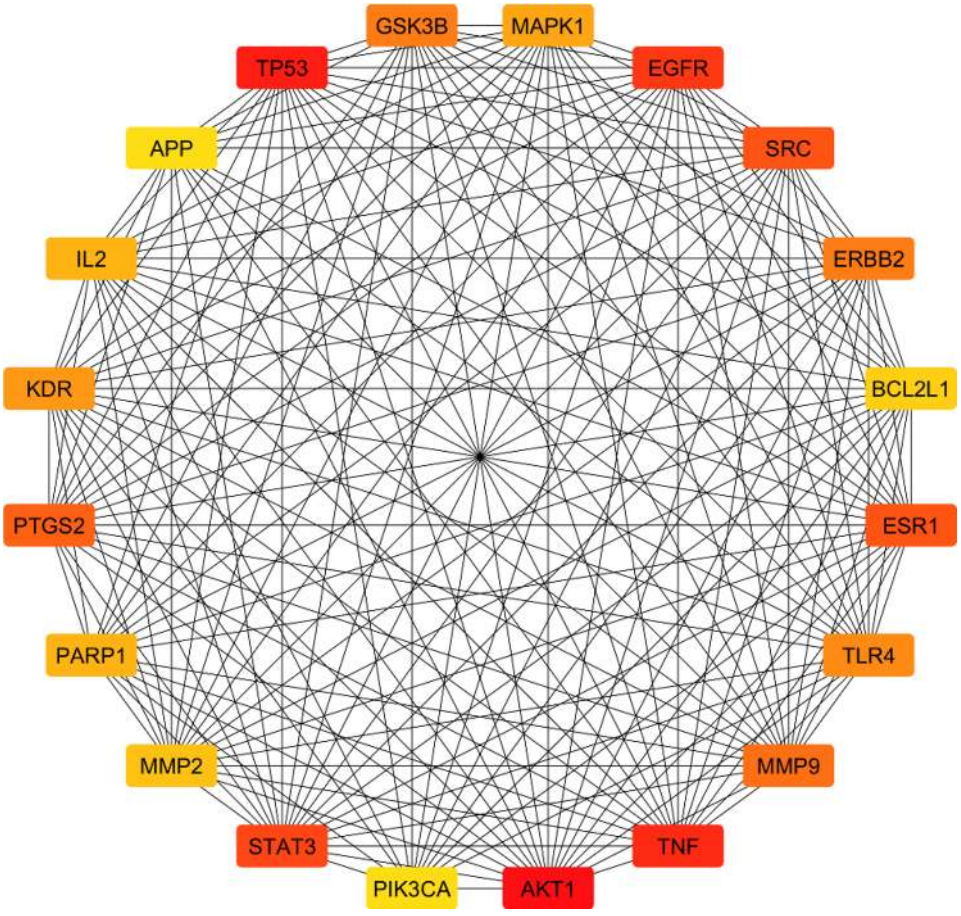

Fig. 8 Cytoscape-generated protein–protein interaction network integrating flavonoid-enriched crude formulations A and B targets with T2DM-associated genes, highlighting the central subnetwork of 20 key nodes identified through CytoHubba analysis

6B1E. Among the bioactive compounds, myricetin (-9.1 kcal/mol) and rutin (-8.9 kcal/mol) were the top bioactive compounds for 1B2Y. For the 3TOP target, myricetin (-8.9 kcal/mol) and quercetrin (-9.1 kcal/mol) had the best energies. Compared with 6B1E, quercetrin (-7.9 kcal/mol) and myricetin (-7.8 kcal/mol) were the most promising. Notably, while the top bioactive compounds displayed less negative binding energies for 1B2Y and 3TOP than did acarbose, their interactions with 6B1E were more favorable than those of the reference compound vildagliptin. Additionally, both myricetin and quercetrin exhibited dual high binding inclinations to a minimum of two protein targets (Fig. 11).

The docking of these compounds to the targets identified by network pharmacology revealed binding ranges of -5.5–9.3, -5.3–7.2, -5.0–7.6 and – 6.7–7.0 kcal/mol for the Akt1, Stat-3, p53, and TNK-alpha targets, respectively, with rutin and quercetrin being the top two docked compounds across the targets (Table S1: supplementary data).

Docking interactions of leading bioactive and reference compounds with T2DM target proteins

The ranked compounds that were selected on the basis of their binding energy and interaction with the catalytic residues of the target proteins were further subjected to interaction analysis (Table 3). From the validation analysis, acarbose was stretched in a binding conformation similar to the extracted conformation in the binding site of 1B2Y, with a bond stabilized by several hydrogen bonds and one hydrophobic contact with Trp59. Myricetin was also stabilized in the binding site by several hydrogen bonds interacting with the same residues as acarbose and via more hydrophobic interactions, including pi-anion interactions with Asp197 and pi-pi stacking with Tyr62 and Trp59. Similarly, rutin was stabilized by several hydrogen bonds and few hydrophobic interactions with His305 (Pi-cation), Asp356 (pi-anion), Trp59 (pi-pi T-shaped and pi-pi stacking), Trp59 (pi-alkyl), His101 (alkyl) and Leu165 (alkyl) (Fig. 12).

Acarbose was stabilized in the active site of 3TOP via 13 hydrogen bonds and few hydrophobic contacts, including pi–sigma interactions with Phe1560 and pi–alkyl interactions with Tyr1251, Phe1559 and Phe1560. Myricetin also formed 9 hydrogen bonds and 6 hydrophobic interactions, including pi-anion interactions with Asp1526, pi-pi T-shaped interactions with Trp1369, Trp1355 and pi-pi stacking with Phe1559 and Phe1560. Quercetrin formed 9 hydrogen bonds and 3 pi-pi T-shaped interactions with Trp1355, Phe1559 and Tyr1251 (Fig. 13). Vildagliptin was stabilized at the binding site of 6B1E with 6 hydrogen bonds, attractive charge contacts with His740, pi-sigma interactions with Phe357, pi-alkyl interactions with Phe357 and pi-cation interactions with Glu206 and Glu205. Myricetin was also stabilized at the binding site by several hydrogen bonds interacting with the same residues as vildagliptin and few hydrophobic contacts, including pi-anion interactions with Glu206 and pi-pi stacking with Phe357. Quercetrin forms hydrogen bonds with several 11 amino acid residues and a pi-anion contact and pi-pi stacking with Phe357 (Fig. 14).

Additionally, the top two compounds (rutin and quercetrin) across the four targets significantly interact with amino acids through a balance of hydrogen, hydrophobic and van der Waals bonds (Fig. 15).

Molecular dynamics

Table 4 summarizes the mean values and standard deviations for all the thermodynamic parameters, whereas Fig. 16 shows the time-resolved parameter profiles. The RMSD trajectories for the 1B2Y complexes indicated system equilibration prior to 10 ns, with minimal structural variation observed postequilibration (Fig. 16a). RMSF measurements were used to assess residue-level flexibility following the binding of myricetin and quercetrin to the 1B2Y active site (Fig. 16b). The top-docked compounds (myricetin and rutin) presented ROG averages comparable to those of acarbose (23.34 Å, 23.33 Å, and 23.29 Å, respectively), suggesting similar compactness (Fig. 16c). While compound binding appeared to influence protein structural stability, the SASA values matched those of acarbose, indicating that no significant unfolding occurred (Fig. 16d). The number of hydrogen bonds remained stable across all the complexes, with the ligand-bound systems maintaining consistent interactions (Fig. 16e). For the TNF-alpha systems, comparing the RMSD of the unbound 2AZ5 and the bound system, rutin appears to stabilize the protein complex slightly better than does quercetrin, as indicated by the lower RMSD (1.48 Å vs. 2.12 Å). With a slightly greater RMSF (1.38 Å) than the unbound 2AZ5 (1.22 Å), 2AZ5_Rutin adds some flexibility. AZ5_Quercetrin (1.14 Å) has less flexibility, indicating that it might more successfully limit residue migrations. Comparable RoG values (~ 15.3 Å) are displayed for all the systems, indicating no appreciable variation in compactness. 2AZ5_Rutin (6497.6 $Å^2$) has a lower SASA than does 2AZ5 (6933.0 $Å^2$), indicating tighter packing when Rutin is bound. Rutin has a greater degree of reduced SASA than 2AZ5_Quercetrin does (6595.1 $Å^2$). Strong binding is shown by the maximum number of H-bonds formed by 2AZ5_Rutin (62.64). 2AZ5_Quercetrin forms 58.05 H-bonds, which are still substantial but fewer than Rutin (Fig. 17).

Binding affinities analysis via MMGBSA

The binding affinities of the top two phytochemicals for protein 1B2Y were quantified via MMGBSA. Compared with the reference compound, myricetin exhibited the most favorable binding affinity (-17.67 ± 6.02 kcal/mol),

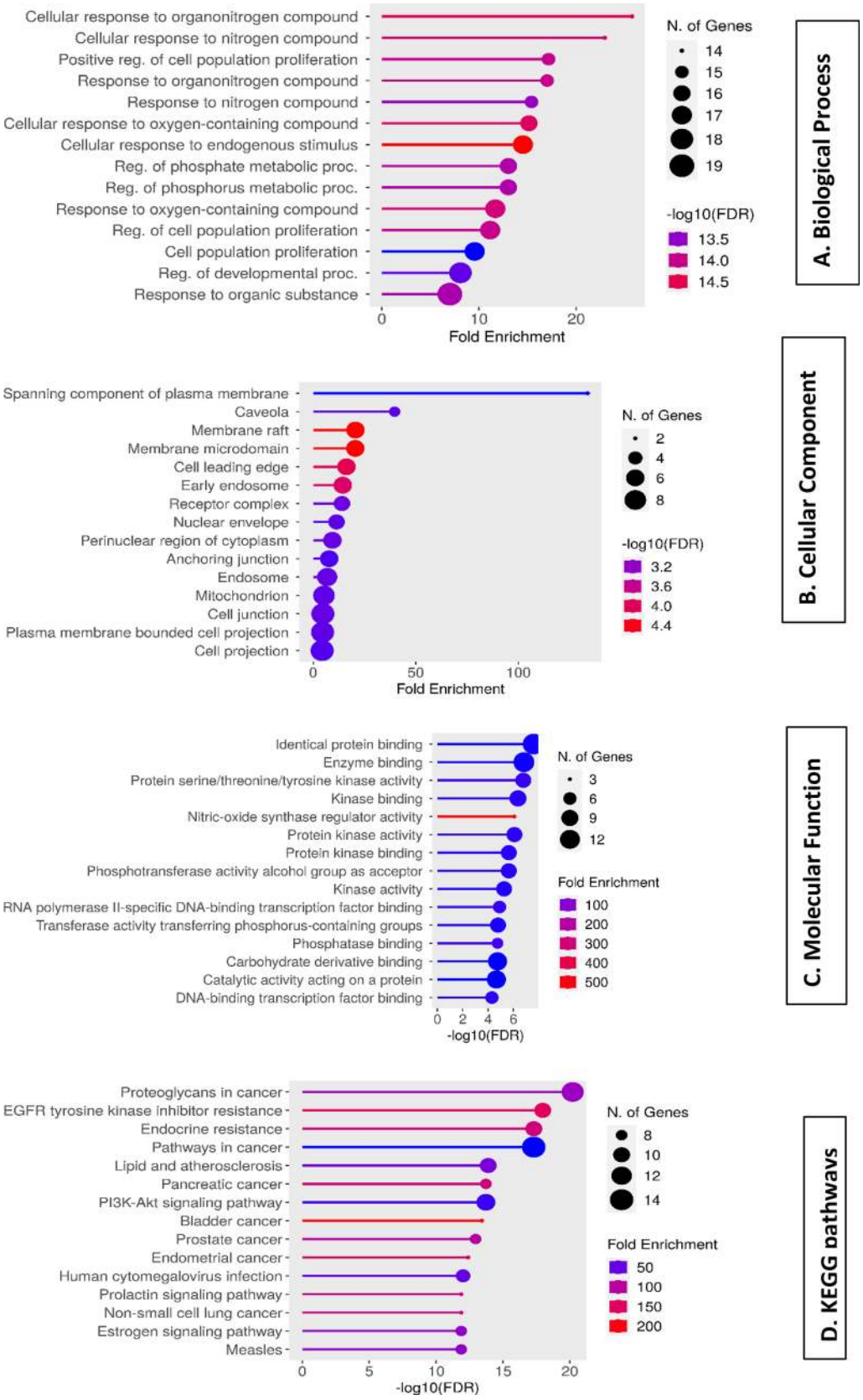

Fig. 9 Summary of enriched pathways and functional annotation terms, including biological processes, cellular constituents, molecular functions, and KEGG pathway analysis

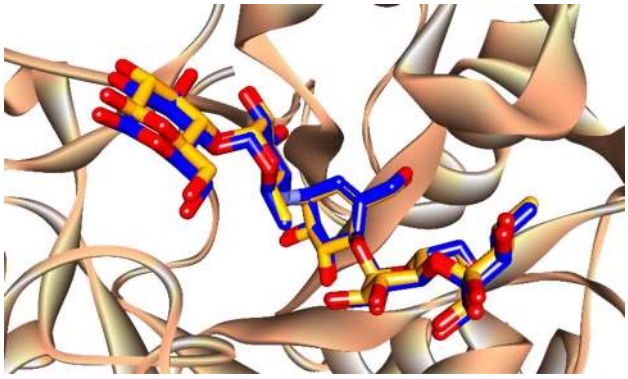

Fig. 10 Superimposition of the conformer with the least minimal binding energy from the docking analysis of acarbose on the conformation of the extracted ligand from 1B2Y. The blue color signifies the docked conformer, whereas the gold color represents the cocrystallized conformation

surpassing acarbose (-10.38 ± 10.63 kcal/mol), with both top candidates demonstrating stronger interactions. Table 5 outlines the energy components contributing to the total binding free energy, whereas Fig. 18 illustrates the residue-specific contributions.

For the TNF-α system, quercetrin and rutin displayed binding energies of -16.36 ± 3.71 and.

-27.97 ± 8.72 kcal/mol, respectively, with their stabilization driven by a balance between van der Waals forces and electrostatic interactions that offset solvation penalties, positioning them as promising candidates for stabilizing 2AZ5.

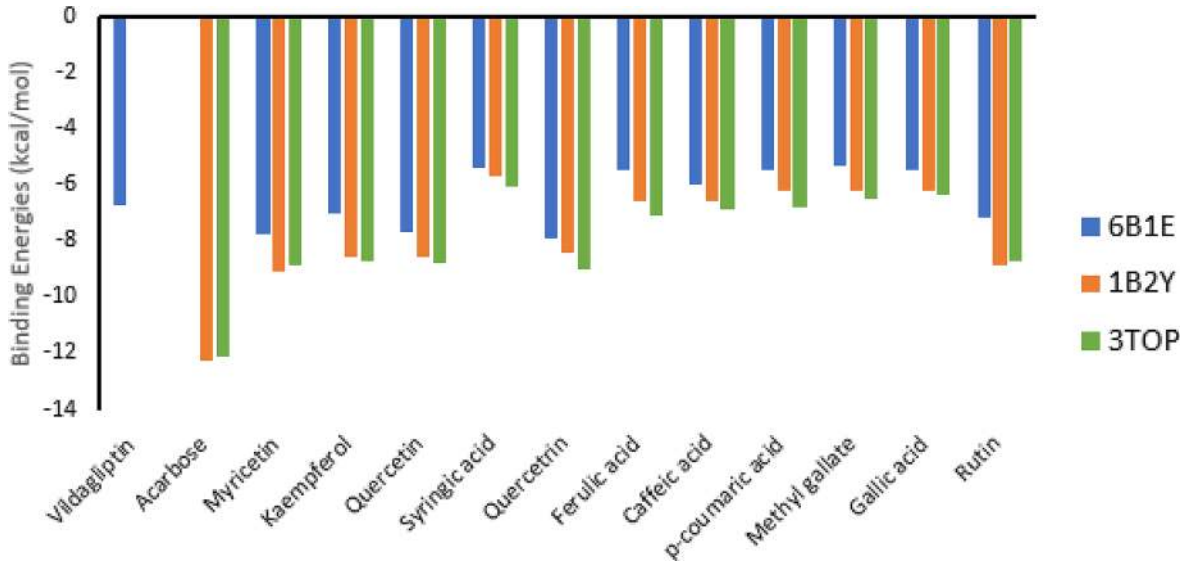

Fig. 11 Binding affinities of identified constituents with key proteins implicated in T2DM

Table 3 Interactions of the top-ranked bioactive constituents of crude formulations A and B with the three target proteins

Compounds	Protein Targets	Hydrogen bonds	Hydrophobic Interaction
		Interacting residues	Interacting residues
Acarbose	1B2Y	Trp59 Gln63 Tyr62 Thr163 GLy306 Thr163 His305 His299 Tyr62 Tyr151 His201 Lys200 Ile235 Arg195 Asp197 Lys200 Glu233 Asp300	Trp59
Myricetin		Gln63 Tyr62 His101 Asp300 His299 Arg195 Ala198 Asp197 Glu233	Trp59 Tyr62 Asp197
Rutin		Ala198 Gln63 Thr163 Tyr62 Tyr151 Trp59 Asp356 Arg195 Val354 Asp300 His299 Asp197	His101 His305 Trp59 Asp356 Tyr62 Leu165
Acarbose	3TOP	Asp1555 Arg1582 Asp1317 His1584 Trp1355 Thr1528 Gln1561 Lys1460 Asp1157 Met1421 Tyr1167 Arg1516 Asp1526	Tyr1251 Phe1559 Phe1560,
Myricetin		Asp1157 Arg1510 Lys1460 Asp1526 His1584 Asp1279 Thr1586 Ile1587 Trp1369	Phe1560 Phe1559, Asp1526 Trp1355 Tyr1251 Pro1159
Quercetrin		Asp1279 His1584 Asp1420 Asp1526 Arg1510 Trp1369 Lys1460 Asp1157	Trp1355 Phe1559 Tyr1251
Vildagliptin	6B1E	Ser630 Asn710 Tyr662 Ser209 His126	His740 Phe357 Phe357 Glu206 Glu205,
Myricetin		Phe357 Val207 Glu206 Arg669 Tyr666 Se630 Tyr662 Tyr631 Arg125 Asn710 Glu205 Tyr547 Phe357	Phe357 Glu206
Quercetrin		Val207 Glu206 Arg669 Tyr662 Asn710 His740 Glu205 Tyr631 Ser630 Tyr547 Arg125	Phe357

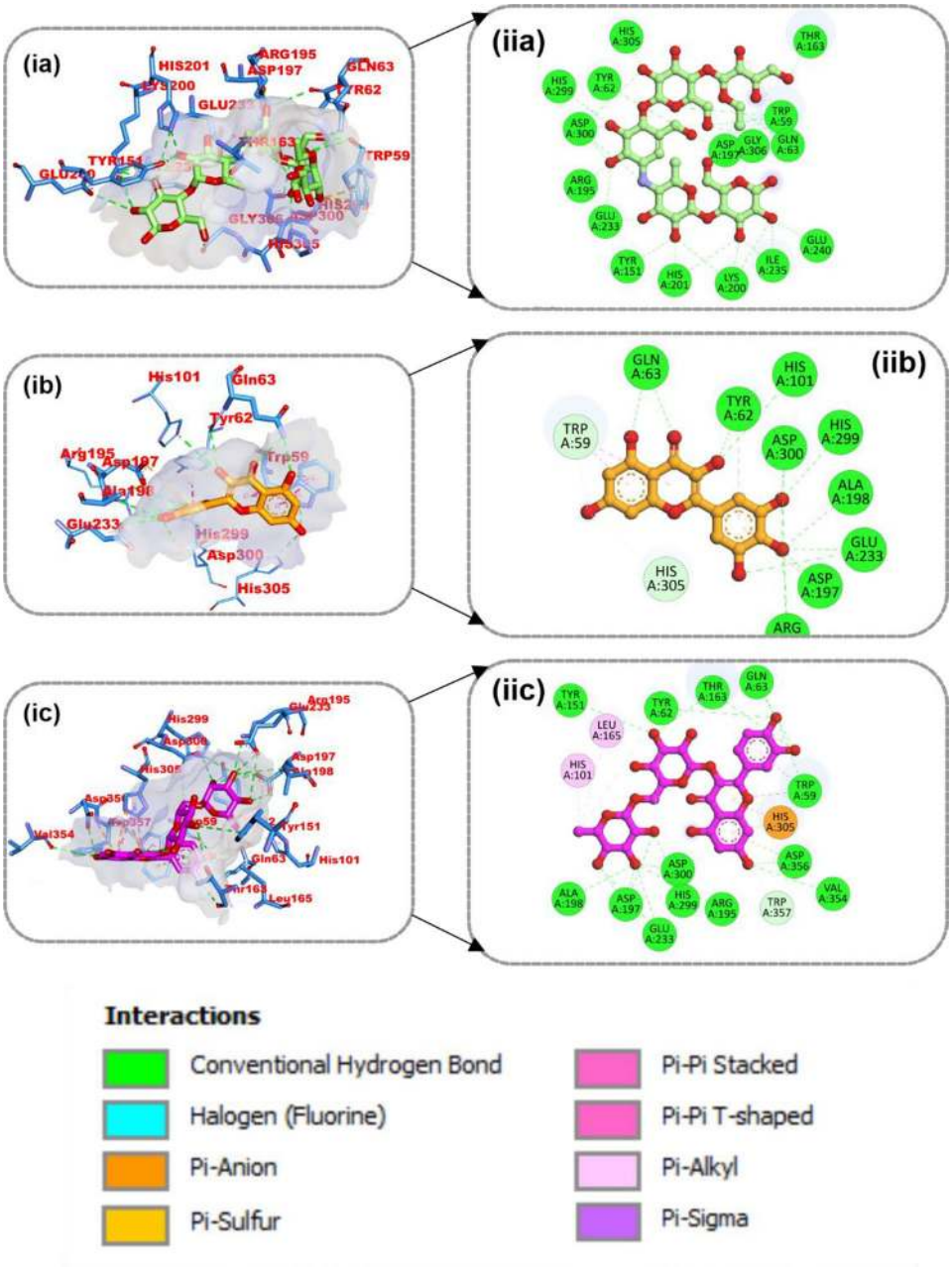

Fig. 12 Top-ranked compounds and acarbose interactions with the amino acid active site of 1B2Y. Sticks are used to represent the ligands. **(i)** 3D and **(ii)** 2D interactions. **(a)** Acarbose, **(b)** myricetin, and (**c**) rutin

Discussion

Globally, populations with diabetes use a variety of plants that have hypoglycemic qualities, depending on historical, cultural, and economic factors [54]. Historically, herbal remedies have been used to treat diabetes and hypertension [55]. Owing to the adverse effects associated with existing antihyperglycemic drugs [56], researchers are actively exploring plant-derived compounds as alternative inhibitors of intestinal α-glucosidase and pancreatic α-amylase, given their lower risk of side effects and potential to lower blood glucose levels [57]. By functioning as enzyme inhibitors, several plants have been used to treat diabetes [58, 59].

Polyphenols are among the most important and common phytochemicals found in medicinal plants [60]. These compounds include tannins, phenolic acids, flavonoids, coumarins, lignans, and stilbenes, among other chemical compounds. Phenolic acids are broadly classified into two main categories: benzoic acids (C6–C7) and cinnamic acids (C6–C3), both of which share a nine-carbon structural framework [61]. Cinnamic acid and its derivatives are synthesized by plants via the shikimate

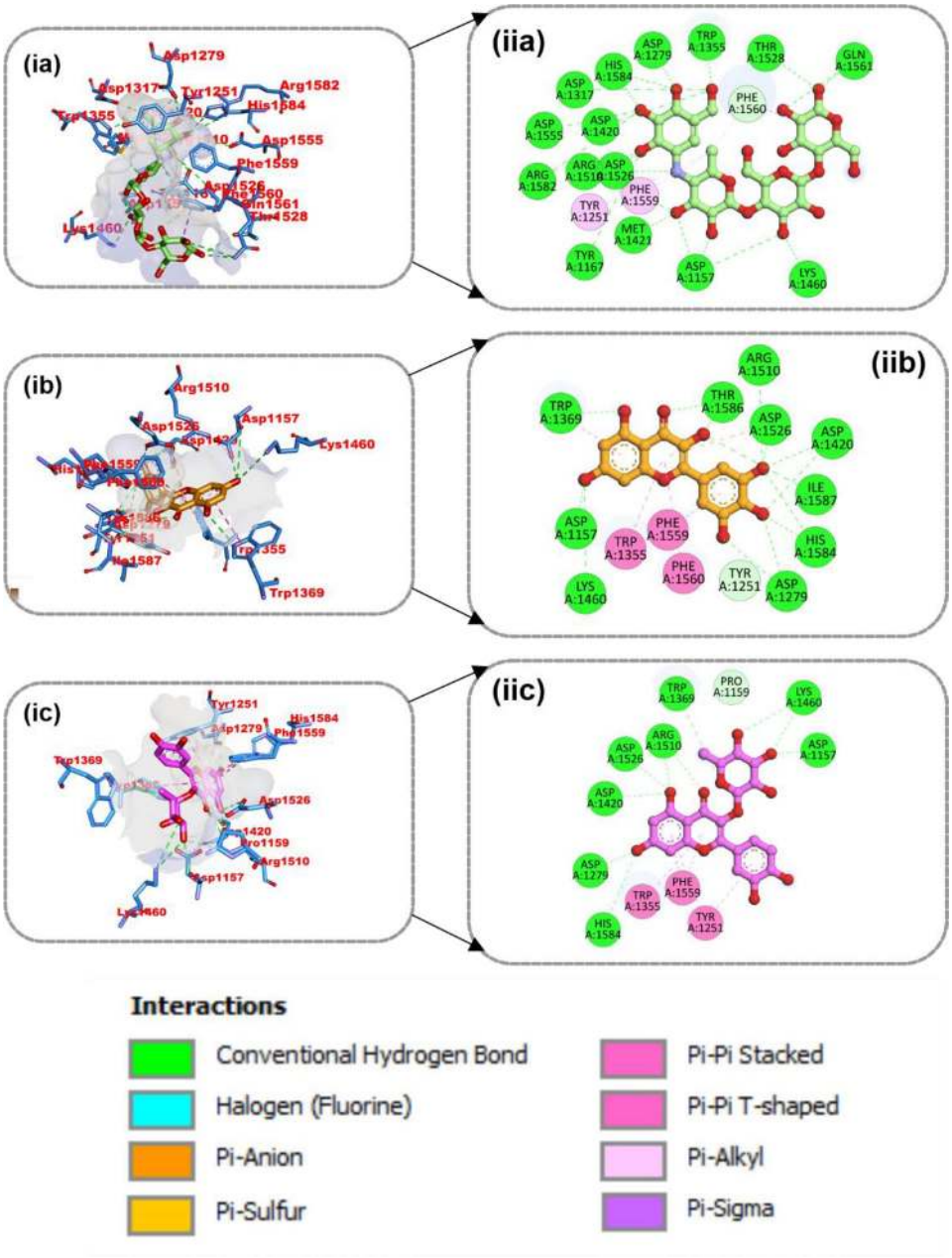

Fig. 13 Visualization of the highest-ranking compounds and the reference inhibitor acarbose docked at the active site of 3TOP, with ligands depicted as stick models. Shown are both (**i**) three-dimensional and (**ii**) two-dimensional interaction diagrams for (**a**) acarbose, (**b**) myricetin, and (**c**) quercetrin

pathway [62, 63]. Studies on their pharmacokinetics and bioavailability indicate that the limited presence of cinnamic acid and its derivatives in the bloodstream is likely a result of their rapid elimination, extensive metabolic processing, and/or poor absorption [64, 65]. These variables may be insufficient to produce the desired biological effects needed to prevent chronic illnesses. The bioavailability and biological effects of cinnamic acid have been enhanced through novel strategies that include the derivatization and combination of these derivatives at various ratios [66, 67].

Formulation A may have a stronger antidiabetic effect because it contains syringic acid, known for its antidiabetic effect [68], along with derivatives of cinnamic acid. Cinnamic acid and its derivatives exert their effects by binding to the active sites located at the C- and N-terminal regions of α-amylase and α-glucosidase [69, 70]. The inhibitory action of cinnamic acid on α-glucosidase is strengthened when hydroxyl or methoxy groups are present [71]. The methoxy group was more potent than the hydroxyl group [72]. Additionally, DPP-IV activity is inhibited by cinnamic acid and its derivatives [69, 73, 74].

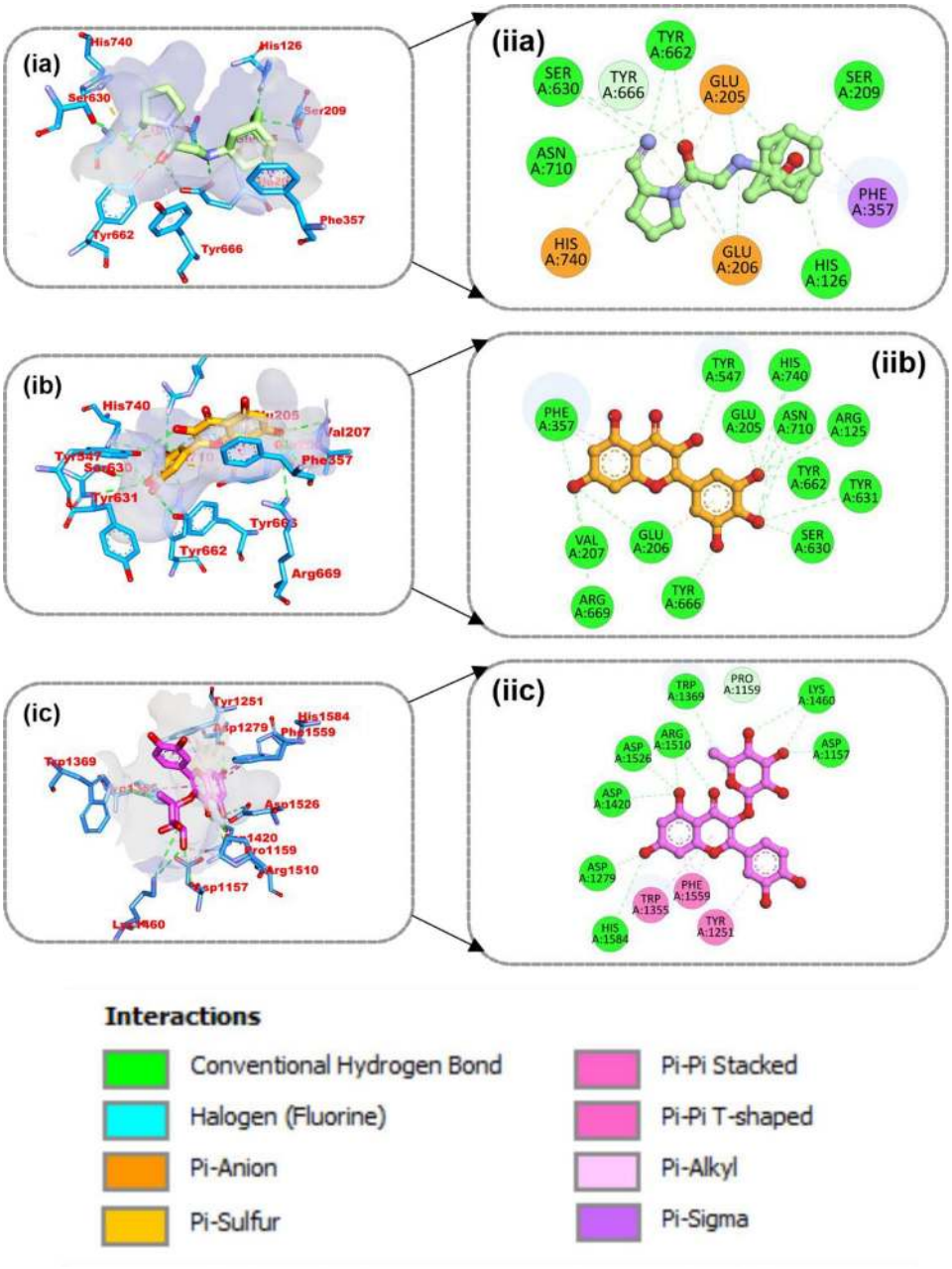

Fig. 14 Visualization of the highest-ranking compounds and the reference inhibitor vildagliptin docked at the active site of 6B1E, with ligands depicted as stick models. Shown are both (**i**) three-dimensional and (**ii**) two-dimensional interaction diagrams for (**a**) vildagliptin, (**b**) myricetin, and (**c**) quercetrin

More recently, caffeic acid has been found to inhibit DPP-IV activity [75, 76]. Therefore, the substantial inhibitory effects of formulation A on α-amylase, α-glucosidase, and DPP-IV may be attributed to syringic acid and other flavonoids, which possess two methoxy groups at the meta position of the cinnamic acid skeleton.

Toxicological investigations of a few cinnamic acid derivatives, which were also present in formulations A and B, demonstrated the compounds' nontoxic qualities, indicating their appropriateness for in vivo usage [77, 78]. The ability of cinnamic acid derivatives to suppress the proliferation of cells with aberrant p53 while sparing other cells was shown by Ogunlakin et al. [79]. Marangi et al. [80]. also assessed the possible cytotoxic effects of kiwi berry leaf extracts rich in cinnamic acid derivatives on HFF-1 cells. A viability of 66% was reported in HFF-1 cells at the highest concentration tested (500 µg/mL) after testing a range of concentrations (15.63 µg/mL–500 µg/mL). Furthermore, cinnamic acid derivatives stimulate pancreatic cells and sciatic nerve regeneration [69, 81, 82]. Consistent with these studies, the crude formulations did not exhibit cytotoxicity in HFF cells at

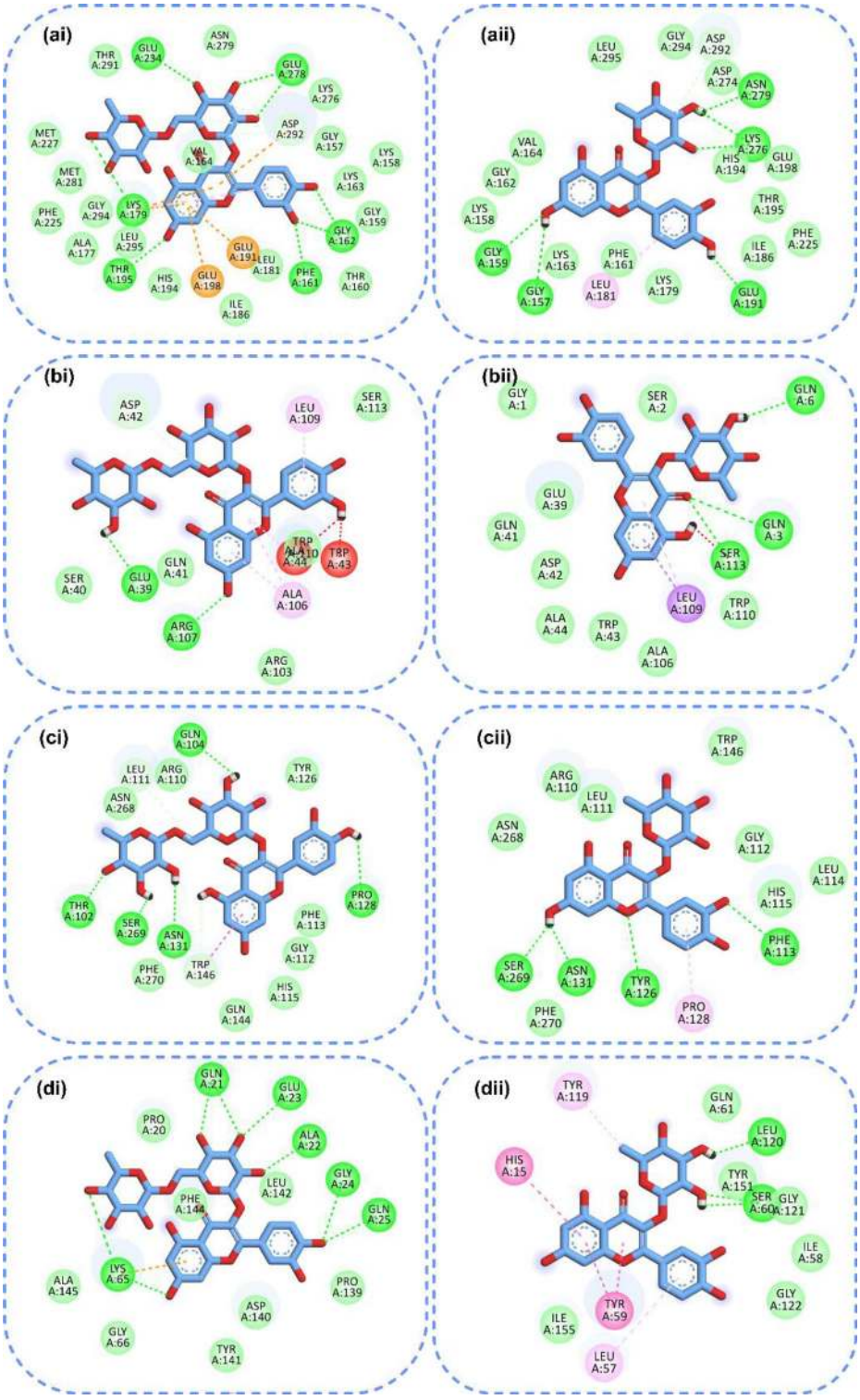

Fig. 15 Top-ranked compounds, (**i)** rutin, **(ii)** quercetrin, from the docking analysis of compounds that interact with the amino acids **(a)** Akt1, **(b)** STAT-3, (**c)** P53, and **(d)** TNF-alpha. Sticks are used to represent the ligands

the indicated concentrations. Taken together, these findings demonstrate the potentially beneficial application of formulations rich in cinnamic acid derivatives and other flavonoids in the management of diabetes. However, investigations of the toxicity of these formulations via in vivo methods are needed.

In contemporary drug design and identification of bioactive compounds, network pharmacology,

Table 4 Mean and standard deviation values for key parameters from the MDS trajectories of the top-ranked compound–target complexes

Complexes	Thermodynamic parameters				
	RMSD (Å)	RMSF (Å)	RoG (Å)	SASA (Å^2)	H-Bonds
1B2Y_Acarbose	1.55 ± 0.26	0.86 ± 0.54	23.3 ± 0.08	21386.1 ± 439.8	122.7 ± 9.38
1B2Y_Myricetin	1.54 ± 0.22	0.85 ± 0.47	23.3 ± 0.09	21156.5 ± 362.4	123.7 ± 9.12
1B2Y_Rutin	1.43 ± 0.26	0.82 ± 0.52	23.2 ± 0.08	20831.0 ± 426.3	127.2 ± 8.85
2AZ5	1.57 ± 00.2	1.22 ± 0.52	15.3 ± 0.10	6933.0 ± 175.6	56.16 ± 4.89
2AZ5_Rutin	1.48 ± 0.22	1.38 ± 0.67	15.3 ± 0.09	6497.6 ± 247.5	62.64 ± 62.6
2AZ5_Quercetrin	2.12 ± 0.27	1.14 ± 0.54	15.2 ± 0.08	6595.1 ± 171.3	58.05 ± 4.99

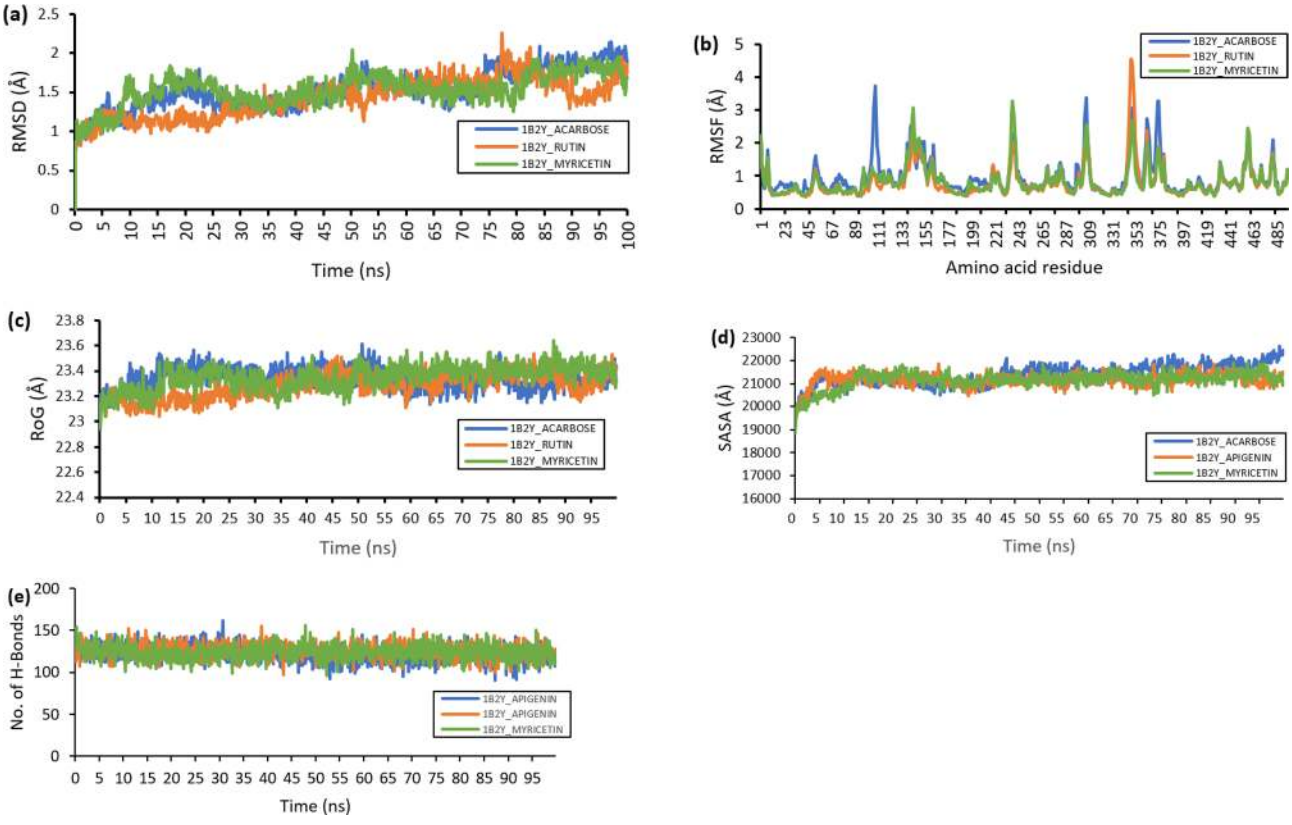

Fig. 16 Molecular dynamics trajectory analysis of 1B2Y complexes

molecular docking, and molecular dynamics are essential approaches that offer unique but complementary perspectives on the intricate procedures involved in drug discovery and development. This combination makes it easier to find novel drug candidates, optimize current medications, and comprehend pharmacological mechanisms [83].

Furthermore, we investigated how to use network pharmacology, molecular docking, and molecular simulation to evaluate the potential bioactive components identified in formulations against T2DM in complex situations. A total of 3238 genes linked to T2DM were identified from various databases, and screening of the bioactive compounds yielded 188 targets, with 119 overlapping genes that were common to T2DM genes and targets associated with bioactive compounds. In the PPI network, target proteins, a complex network of bioactive compounds and T2DM targets, reflect multicomponent properties. With a PPI enrichment value of less than 1.0×10^{-16}, an average number of generated edges and the expected number of edges, the network had substantially more interactions than predicted, indicating that the proteins are biologically related as a group [84].

Among the 119 overlapping genes that were further analyzed via Cytoscape, the most enriched targets were the inflammatory markers TNF (tumor necrosis factor), TP53 (tumor protein 53) [85], AKT1 (Akt serine/threonine kinase 1) [86], and STAT3 (signal transducer and activator of transcription 3) [87], which are essential for cellular functions such as metabolism, apoptosis,

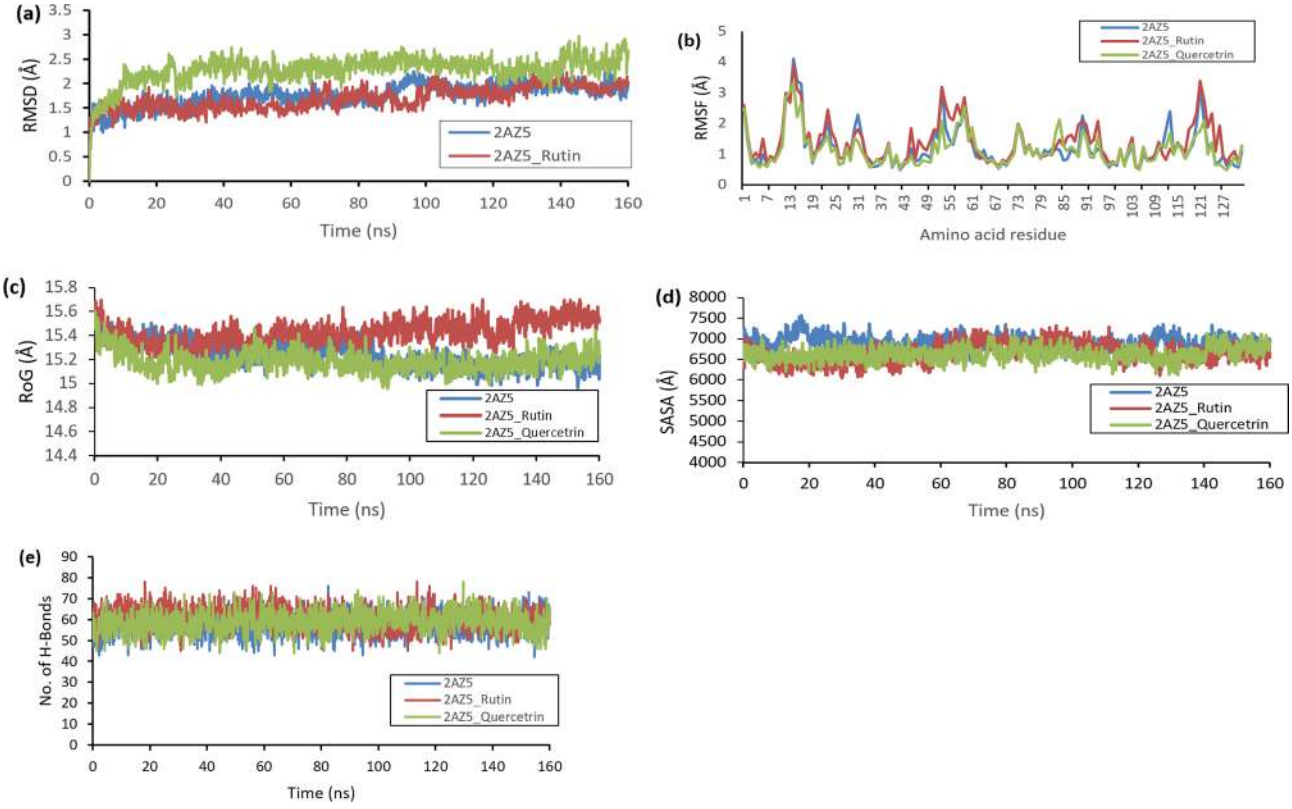

Fig. 17 Molecular dynamics trajectory analysis of TNF-alpha complexes

Table 5 Mean and standard deviation values of the binding free energy components (kcal/mol) for the top phytochemical–target interactions

SYSTEM	$\Delta_{VDWAALS}$	Δ_{EGB}	Δ_{EEL}	Δ_{GGAS}	Δ_{ESURF}	Δ_{GSOLV}	Δ_{TOTAL}
1B2Y_ acarbose	-10.54 ± 8.68	18.48 ± 19.78	-16.03 ± 20.78	-26.64 ± 27.76	-2.28 ± 1.83	16.23 ± 18.06	-10.38 ± 10.63
1B2Y_Rutin	-14.15 ± 2.88	-16.36 ± 12.3	21.95 ± 6.31	-2.73 ± 0.42	-30.48 ± 11.9	19.23 ± 6.04	-11.34 ± 7.09
1B2Y_Myricetin	-23.48 ± 4.98	35.10 ± 9.61	-26.14 ± 15.11	-49.62 ± 14.67	-3.14 ± 0.65	31.93 ± 9.29	-17.67 ± 6.02
2AZ5_Rutin	-28.25 ± 4.64	43.77 ± 15.15	-39.38 ± 21.53	-67.63 ± 22.04	-4.11 ± 0.72	39.66± 14.61	-27.97 ± 8.72
2AZ5_Quercetrin	-24.25 ± 3.57	12.24 ± 4.23	-1.34 ± 5.04	-25.60 ± 5.90	-3.01 ± 0.43	9.23 ± 4.15	-16.36 ± 3.71

inflammation, and cell survival. In addition to insulin resistance and diabetic complications, these targets have been linked to the pathophysiology of diabetes, particularly type 2 diabetes (T2D) [88, 89]. Other targets, including MAPK1, GSK3B, PARP1, MMP2, PIK3CA, MMP9, TLR4, and ESR1, also have different implications in the pathogenesis of T2D. For example, by interfering with insulin receptor signaling, overactivation of MAPK1 signaling leads to insulin resistance. Serine phosphorylation of insulin receptor substrates (IRSs) due to elevated MAPK1 activity can disrupt insulin signal transduction [90]. Compounds that inhibit the MAPK1 pathway reduce the incidence of T2D. Furthermore, GSK3B is a serine/threonine kinase involved in regulating various cellular processes, including glucose metabolism and insulin signaling. GSK3B influences insulin sensitivity and prevents the production of glycogen. Increased GSK3B activity in type 2 diabetes prevents the liver and muscles from storing glycogen, which leads to insulin resistance [91]. PARP1 is involved in cellular stress responses and DNA repair. Overactivation of PARP1 in beta-cells causes apoptosis and exacerbates insulin secretion in type 2 diabetes. It has been demonstrated that PARP1 inhibition enhances glucose homeostasis and protects against beta-cell death [92].

The functions of bioactive chemicals have focused primarily on cellular responses and the response to nitrogen, oxygen-containing, and organonitrogen compounds on the basis of our biological process (BP) findings. Both cellular stress responses and nitrogen metabolism are intricately associated with the pathogenesis of T2D, particularly in the context of insulin resistance, beta-cell dysfunction, inflammation, and metabolic abnormalities [93]. T2D is characterized by chronic low-grade inflammation, which triggers an array of cellular signaling pathways, such as those comprising the mitogen-activated

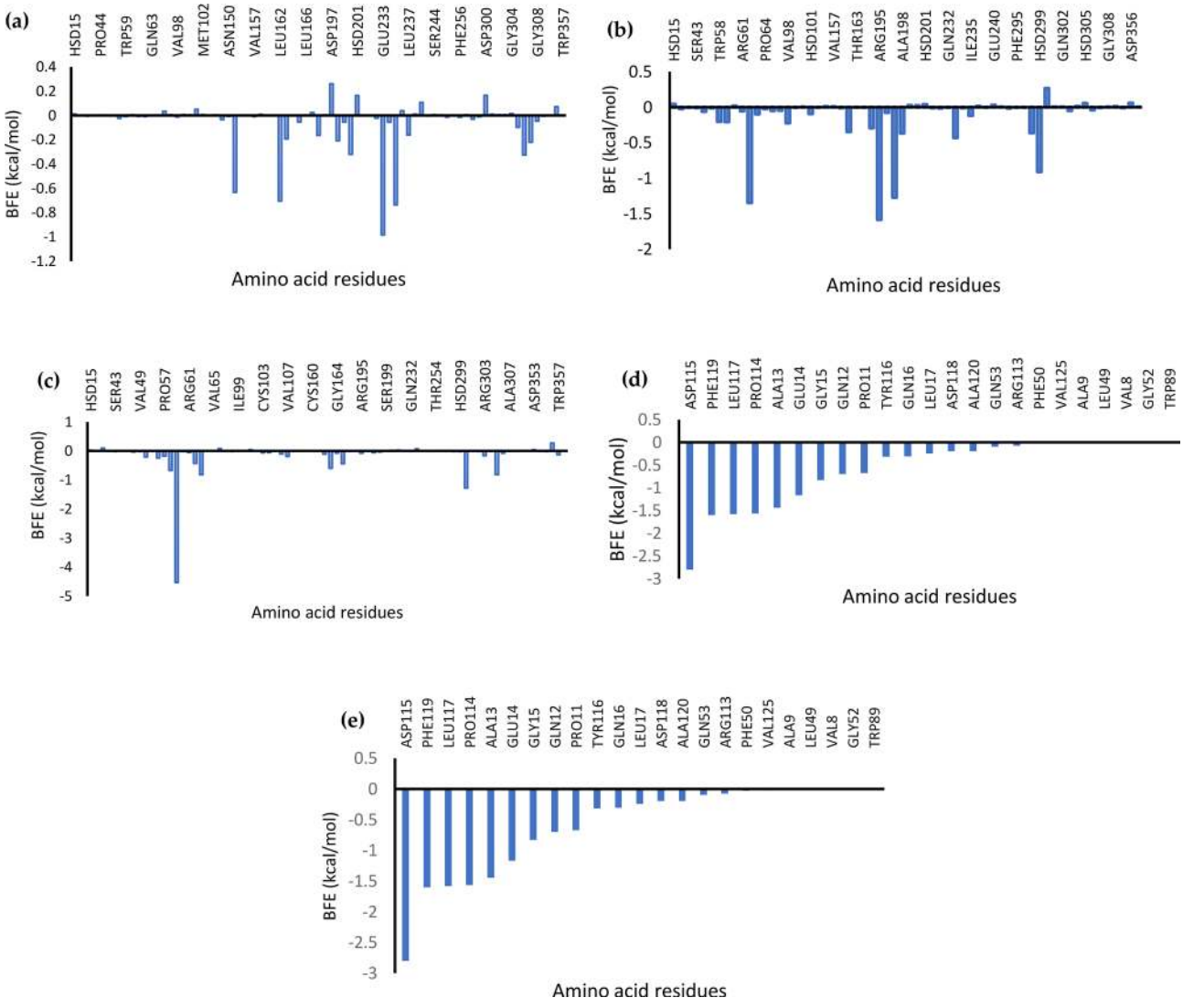

Fig. 18 MM-GBSA plot of the contributing amino acid residues of (**a**) 1B2Y_acarbose, (**b**) 1B2Y_rutin, (**c**) 1B2Y_myricetin, (**d**) 2AZ5_rutin, and (**e**) 2AZ5_quercetrin

protein kinase (MAPK) and nuclear factor kappa-light-chain-enhancer of activated B cells (NF-κB) pathways. These pathways impede insulin signaling by promoting the production of proinflammatory cytokines, including IL-6 (interleukin-6) and TNF-α (tumor necrosis factor-alpha). The decreased ability of insulin to promote glucose absorption into muscle and adipose tissue, which results in increased blood glucose levels, is a hallmark of insulin resistance [94, 95]. The control of the urea cycle, protein synthesis, and amino acid metabolism are the main mechanisms underlying the response to nitrogen. The ratio of branched-chain amino acids (BCAAs) to essential amino acids is not balanced in type 2 diabetes. T2D patients frequently have elevated blood levels of BCAAs, such as leucine, isoleucine, and valine [96]. By encouraging the activation of mTOR (mechanistic target of rapamycin) and decreasing insulin sensitivity in muscle and adipose tissue, high levels of BCAAs can disrupt insulin signaling [97].

With respect to cellular processes, the most enriched terms were the following: spanning components of the plasma membrane, caveolae, membrane rafts, and membrane microdomains. For Molecular Function (MF), the most enriched terms included identical protein binding, enzyme binding, protein/threonine/serine/tyrosine kinase activity, catalytic activity acting on protein, and carbohydrate derivative binding. Understanding the molecular causes of insulin resistance, inflammation, and metabolic dysfunction in type 2 diabetes (T2D) requires an understanding of the spanning components of the plasma membrane, caveolae, membrane rafts, and membrane microdomains [98]. Insulin receptor binding occurs in the plasma membrane, where it triggers signaling pathways, such as the PI3K–Akt pathway, which

in turn triggers mTOR. This signaling is compromised in insulin resistance, which leads to aberrant metabolic reactions and decreased glucose absorption [99]. The interaction of the bioactive compounds may interfere with this cellular process, thereby reducing the blood glucose concentration by increasing glucose absorption. KEGG pathway enrichment analysis revealed that the bioactive compounds were associated with several key pathways, including those related to cancer, EGFR tyrosine kinase inhibitor resistance, lipid metabolism and atherosclerosis, endocrine resistance, and the PI3K−Akt signaling pathway. Among these pathways, the PI3K−Akt pathway plays a central role in regulating essential biological processes such as protein synthesis, insulin sensitivity, glucose metabolism, and cell growth and survival. Dysregulation of this pathway is commonly observed in type 2 diabetes, contributing significantly to the development of insulin resistance, elevated blood glucose, and broader metabolic disturbances [99]. An appealing therapeutic approach for enhancing insulin sensitivity and controlling type 2 diabetes is to target elements of the PI3K–Akt signaling pathway, and the interaction between the bioactive compounds and this pathway may be a possible mechanism of the antidiabetic properties of the formulation.

Molecular docking was performed to assess the interaction between bioactive compounds in the formulation and the target enzymes that were used to assess the antidiabetic effects of the formulation. Validation of the molecular docking protocol has become an important step before conducting the main analysis with the aim of reducing errors associated with the process [100]. In the present study, the obtained docked conformations were close to those of the native ligands, indicating a proper protocol for screening the bioactive components.

Interestingly, the top two bioactive compounds for alpha-amylase, which are myricetin [101, 102] and rutin, have been reported to have anti-T2D activities. Similarly, the top two ranked compounds for alpha-glucosidase activity are myricetin [103, 104], and quercitrin has been reported to have alpha-glucosidase inhibitory activity. Quercitrin [105] and myricetin [106] have been reported to have anti-DPP4 inhibitory activities. Hence, these compounds, in part or in synergetic activities, may have been responsible for the inhibitory activities of the enzymes that were studied *in vitro*.

Structural stability assessment of the top bioactive complexes with 1B2Y was performed by monitoring the RMSD, radius of gyration (ROG), solvent accessible surface area (SASA), and hydrogen bond formation during MD simulations compared with those of the acarbose-bound reference system. Root mean square deviation (RMSD) trajectories quantified structural divergence from initial conformations over time, with values below 3 Å indicating stable ligand–protein interactions, as established in prior studies [107]. According to the mean RMSD values, the myricetin complex presented a close mean value compared with that of acarbose, whereas the rutin complex presented a lower mean RMSD than did the acarbose. RMSD trajectory analysis suggested that the binding of myricetin and rutin did not adversely affect the thermal or structural stability of the protein; in fact, rutin formed a more stable complex than the reference inhibitor, acarbose [108].

The RMSF values, which measure the average atomic and residue fluctuations during the simulation, reflect the capacity of these components to form stable intra- and intermolecular interactions within the protein. Lower fluctuations, especially at the active site, indicate stronger binding and higher ligand affinity [108]. In this study, the top-ranked ligands did not induce additional residue fluctuations compared with the reference compound. The fluctuation at the end of the spectrum is due to terminal fluctuations. The greatest fluctuation was observed for amino acid residue 111 in the acarbose complex system, but this fluctuation was minimal in the myricetin and rutin complexes. Similarly, compared with the acarbose system, the myricetin and rutin complexes presented minimal fluctuations around amino acid residues 309 and 375.

The radius of gyration (ROG) serves as a metric for assessing the compactness of a complex throughout a molecular dynamics simulation; lower ROG values indicate a more stable and tightly packed structure. Analysis revealed that the binding of the top-docked compounds did not compromise the protein's structural integrity or promote unfolding. The solvent accessible surface area (SASA), which reflects changes in protein folding and overall surface exposure, remained comparable between the top-docked complexes and the acarbose-bound reference, further supporting the notion that protein unfolding did not occur [109]. Protein stability during simulation is also influenced by the presence and consistency of intramolecular hydrogen bonds. Throughout the simulation, the average number of hydrogen bonds remained steady across all complexes, suggesting that ligand binding did not disrupt the protein's structural stability [107].

For the TNF-alpha system, rutin demonstrates enhanced stability (lower RMSD, reduced SASA), a high number of H-bonds, and moderate flexibility, implying stabilization of the protein while maintaining strong and possibly more stable interactions with the protein. Despite having a greater RMSD, quercetrin nevertheless strongly binds through H-bonds and has a lower SASA, which decreases the flexibility (RMSF). Quercetrin might add more structural variability than rutin does (89, 109).

The binding free energy quantifies the energy difference between the bound and unbound components of a complex (ligand and receptor); the greater the negative value is, the higher the ligand's affinity for the protein [109]. In the early phases of drug discovery and development, binding free energy estimates offer thorough information on the binding processes of the top docked compounds [110]. The residues interacting during static docking were found to be primarily involved in contributing to the total binding free energy, further indicating the ability of the compounds to bind strongly to the targets, probably offering a modulatory effect.

Future directions for this research will be to continue exploring indigenous herbal formulations to identify new bioactive compounds with potential antidiabetic properties, conduct in vivo studies to validate the efficacy and safety of promising formulations identified through in vitro and computational studies, and design and implement clinical trials to assess the therapeutic potential of these formulations in human subjects. In addition, the likelihood that these formulations will progress to animal studies and clinical trials will depend on securing funding and resources for extensive research, meeting regulatory requirements and obtaining approval from relevant authorities necessary before proceeding to clinical trials, and collaborating with academic institutions, research organizations, and pharmaceutical companies can facilitate the progression of these formulations. This study has several limitations, one of which is that the results from computational models need to be validated through in vivo studies to ensure reliability. Furthermore, several limitations of network pharmacology models range from their inability to be used in real-world biological systems because they are highly complex, with numerous interacting pathways and feedback mechanisms. Computational predictions on the basis of data from model organisms may not always translate directly to human biology owing to species-specific differences in molecular pathways and drug responses. In addition, computational models can generate hypotheses; these predictions require experimental validation through in vitro and in vivo studies to confirm their relevance and accuracy.

Conclusion

This study highlighted the potential of herbal formulations containing *B. vulgaris* leaves and roots, *P. americana* seeds, and *S. aromaticum* in the management of T2DM. By employing a comprehensive approach that combines network pharmacology, in vitro enzyme assays, and molecular docking analyses, the formulations demonstrated notable inhibitory activity against critical carbohydrate-metabolizing enzymes, including α-amylase and α-glucosidase. These findings are further substantiated by identifying critical protein targets and pathways involved in diabetes management, which suggests a multitarget mechanism of action that aligns with the principles of African traditional medicine.

While the formulations displayed promising bioactivities, we acknowledge the limitations of relying on in vitro and computational models. Furthermore, future studies should include in vivo validation to assess the pharmacokinetics, toxicity, and efficacy in biological systems. Additionally, clinical trials are essential to confirm their therapeutic potential and translational viability.

Our findings bridge the gap between traditional knowledge and modern biomedical research, emphasizing the value of African traditional medicine in addressing unmet clinical needs. By exploring synergistic phytochemical interactions and employing advanced computational and experimental methods, this work lays a foundation for the development of new, plant-based therapies for diabetes.

Abbreviations

ACM	African traditional medicine
BP	Biological process
DM	Diabetes mellitus
DMEM	Dulbecco's modified Eagle's medium
DPP-IV	Dipeptidyl peptidase IV
EGFR	Estimated glomerular filtration rate
GO	Gene Ontology
HFFs	Human foreskin fibroblasts
HPLC-DAD	High-performance liquid chromatography: diode-array detection
KEGG	Kyoto Encyclopedia of Genes and Genomes
LGMDs	Lipid and glucose metabolic disorders
MFs	Molecular functions
MMGBSA	Molecular mechanics generalized surface area
PI3K/Akt	Phosphoinositide 3-kinase/protein kinase B
PPI	Protein–protein interaction
RMSD	Root mean square deviation
RMSF	Root mean square fluctuation
ROG	Radius of gyration
SASA	Surface accessible surface area
TCM	Traditional complementary medicine
T2DM	Type 2 diabetes mellitus

Supplementary Information

The online version contains supplementary material available at https://doi.org/10.1186/s12906-025-04980-1.

Supplementary Material 1

Acknowledgements

The authors acknowledge Bowen University Grant Research (BURG/2024/006) for funding the research. Dr. Oluwafemi Ojo has been co-funded by the European Union's Horizon Europe Framework Programme for Research and Innovation 2021-2027 under the Marie Sklodowska-Curie action grant agreement No. 101126611.

Author contributions

The study was conceptualized and designed by the OAO. The first draft was written by OAO, GAG, and ODA. OAO, OAAO, DIA, AAO, ADO, TEO, and OSA conducted the experiments. OAO and GAG looked at and analyzed the information. OSA oversaw the experiment. OAO, GAG, ODA, OAAO, DIA, AAO, ADO, TEO, and OSA reviewed the final draft of the manuscript. The manuscript's final form was approved by all the authors.

Funding
This study received financial support from Bowen University through the Bowen University Research Grant (BURG), Grant No. BURG/2024/006, for the period 2023–2024.

Data availability
The datasets generated and/or analyzed during the current study are available in the Mendeley data repository, (Ojo, Oluwafemi Adeleke; Ogunlakin, Akingbolabo; Ajayi-Odoko, Omolola; Gyebi, Gideon; Ayokunle, Damilare; Olanrewaju, Adesoji; Agbeye, Oluwatobi; Ogunwale, Emmanuel; Adeyemi, Oluyomi (2024), "Bioprospection of indigenous herbal formulations for diabetes care via in vitro studies", Mendeley Data, V1, https://doi.org/10.17632/6xw67gtbgc.1). In addition, all data generated or analysed during this study are included in this published article [and its supplementary information files /Tables S4–S7].

Declarations

Ethics approval and consent to participate
We confirm that all procedures utilized in this study were approved by the Research Ethics Committee of Bowen University, including the use of *B. vulgaris* leaves and roots, *Persea americana* seeds, and *Syzygium aromaticum* buds, which were conducted in accordance with the relevant institutional, national, and international guidelines and legislation.

Consent for publication
Not applicable.

Competing interests
The authors declare no competing interests.

Author details
[1]Research Centre for Integrative Physiology and Pharmacology, Institute of Biomedicine, University of Turku, Turku, Finland
[2]Phytomedicine, Molecular Toxicology, and Computational Biochemistry Research Group, Biochemistry Programme, Bowen University, Iwo 232102, Nigeria
[3]Microbiology Programme, Bowen University, Iwo 232102, Nigeria
[4]Department of Biotechnology and Food Science, Faculty of Applied Sciences, Durban University of Technology, P.O. Box 1334, Durban 4000, South Africa
[5]Pure and Applied Biology Programme, Bowen University, Iwo 232102, Nigeria
[6]Chemistry and Industrial Chemistry Programme, Bowen University, Iwo 232102, Nigeria
[7]Animal Science Programme, Bowen University, Iwo 232102, Nigeria

Received: 5 August 2024 / Accepted: 17 June 2025
Published online: 03 July 2025

References

1. Chen L, Chen XW, Huang X, Song BL, Wang Y, Wang Y. Regulation of glucose and lipid metabolism in health and disease. Sci China Life Sci. 2019;62(11):1420–58.
2. Rana S, Ali S, Wani HA, Mushtaq QD, Sharma S, Rehman MU. Metabolic syndrome and underlying genetic determinants—a systematic review. J Diabetes Metabolic Disorders. 2022;21(1):1095–104.
3. Chatterjee S, Khunti K, Davies MJ. Type 2 diabetes. Lancet. 2017;389(10085):2239–51.
4. Kahn SE, Cooper ME, Del Prato S. Pathophysiology and treatment of type 2 diabetes: perspectives on the past, present, and future. Lancet. 2014;383(9922):1068–83.
5. Demir S, Nawroth PP, Herzig S, Ekim Ustünel B. Emerging targets in type 2 diabetes and diabetic complications. Adv Sci. 2021;8(18):e2100275.
6. American Diabetes Association. 9. Pharmacologic approaches to glycemic treatment: Standards of medical care in diabetes—2019. Diabetes Care. 2018;42(1):S90–102.
7. Yuan H, Ma Q, Cui H, Liu G, Zhao X, Li W, Piao G. How can synergism of traditional medicines benefit from network pharmacology? Molecules. 2017;22(7):1135.
8. Booth Z, van Vuuren SF. The combined use of African natural products and conventional antimicrobials: an alternative tool against antimicrobial resistance. In: Abia ALK, Essack SY, editors. Antimicrobial research and one health in Africa. Cham: Springer; 2023.
9. Bnouham M, Ziyyat A, Mekhfi H, Tahri A, Legssyer A. Medicinal plants with potential antidiabetic activity—a review of ten years of herbal medicine research (1990–2000). Int J Diabetes Metabolism. 2006;14:1–25.
10. Pezzani R, Salehi B, Vitalini S, Iriti M, Zúñiga FA, Sharifi-Rad J, Martorell M, Martins N. Synergistic effects of plant derivatives and conventional chemotherapeutic agents: an update on the cancer perspective. Medicina. 2019;55(4):110.
11. Schultze E, Collares T, Lucas CG, Seixas FK. Synergistic and additive effects of ATRA in combination with different anti-tumor compounds. Chemico-Biol Interact. 2018;285:69–75.
12. Bashir R, Tabassum S, Adnan A, et al. Bioactive profile, Pharmacological attributes, and potential application of Beta vulgaris. Food Measurement and Characterization. 2024.
13. Sargunam JH. Determination of bioactivity and therapeutic potential of Beta vulgaris (L.) ethanolic leaf extracts. Curr Aspects Pharm Res Dev. 2021;5:25–32.
14. Ojo OA, Agboola AO, Ogunro OB, Iyobhebhe M, Elebiyo TC, Rotimi DE et al. Beet leaf (Beta vulgaris L.) extract attenuates iron-induced testicular toxicity: experimental and computational approach. Heliyon. 2023;9(7).
15. Ojo OA, Amanze JC, Oni AI, Grant S, Iyobhebhe M, Elebiyo TC, et al. Antidiabetic activity of avocado seeds (Persea Americana Mill.) in diabetic rats via activation of PI3K/AKT signaling pathway. Sci Rep. 2022;12(1):2919.
16. Sarmah RN, Gupta PR, Sharma R, Moktan TN, Bhattacharjee A. Persea Americana mill: A brief Pharmacological review. Int J Pharm Sci. 2024;2(5):705–12.
17. Dabas D, Shegog RM, Ziegler GR, Lambert JD. Avocado (Persea americana) seed as a source of bioactive phytochemicals. Curr Pharm Design. 2013;19(34):6133–40.
18. Ojo AB, Gyebi GA, Alabi O, Iyobhebhe M, Kayode AB, Nwonuma CO, et al. Syzygium aromaticum (L.) merr. & l.m.perry mitigates iron-mediated oxidative brain injury via in vitro, ex vivo, and in Silico approaches. J Mol Struct. 2022;1268:133675.
19. Batiha GE, Alkazmi LM, Wasef LG, Beshbishy AM, Nadwa EH, Rashwan EK, Syzygium L (Myrtaceae), editors. Traditional uses, bioactive chemical constituents, pharmacological and toxicological activities. Biomolecules. 2020;10(2):202.
20. Lai X, Wang X, Hu Y, Su S, Li S. Editorial: network Pharmacology and traditional medicine. Front Pharmacol. 2020;11:1194.
21. Zhang P, Zhang D, Zhou W, Wang L, Wang B, Zhang T, et al. Network pharmacology: toward the artificial intelligence-based precision traditional Chinese medicine. Brief Bioinform. 2024;25(1):bbad518.
22. Ojo OA, Gyebi GA, Ezenabor EH, Iyobhebhe M, Emmanuel DA, Adelowo OA, Olujinmi FE, Ogunwale TE, Babatunde DE, Ogunlakin AD, Ojo AB, Adeyemi OS. Exploring beetroot (Beta vulgaris L.) for diabetes mellitus and alzheimer's disease dual therapy: in vitro and computational studies. RSC Adv. 2024;14:19362–80.
23. Araujo-León JA, Cantillo-Ciau Z, Ruiz-Ciau DV, Coral-Martínez TI. HPLC profile and simultaneous quantitative analysis of tingenone and pristimerin in four Celastraceae species using HPLC-UV-DAD-MS. Revista Brasileira De Farmacognosia. 2019;29:171–6.
24. Bouslamti M, Loukili EH, Elrherabi A, El Moussaoui A, Chebaibi M, Bencheikh N, et al. Phenolic profile, inhibition of α-amylase and α-glucosidase enzymes, and antioxidant properties of Solanum elaeagnifolium cav. (Solanaceae): in vitro and in Silico investigations. Processes. 2023;11(5):1384.
25. Bharti SK, Sharma NK, Kumar A, Jaiswal SK, Krishnan S, Gupta AK, et al. Dipeptidyl peptidase IV inhibitory activity of seed extract of Castanospermum australe and molecular Docking of their alkaloids. Topclass J Herb Med. 2012;1:29–35.
26. Adeyemi OS, Ishii K, Kato K. L-tryptophan-titanium oxide nanoparticles showed selective anti-Toxoplasma gondii activity and improved host biocompatibility. Biomed Pharmacother. 2023;162:114597.
27. Kim S, Chen J, Cheng T, Gindulyte A, He J, He S, et al. PubChem 2023 update. Nucleic Acids Res. 2023;51(D1):D1373–80.
28. Daina A, Michielin O, Zoete V, SwissTargetPrediction. Updated data and new features for efficient prediction of protein targets of small molecules. Nucleic Acids Res. 2019;47(W1):W357–64.

29. Gfeller D, Grosdidier A, Wirth M, Daina A, Michielin O, Zoete V. Swiss target prediction: a web server for target prediction of bioactive small molecules. Nucleic Acids Res. 2014;42(W1):W32–8.
30. UniProt. UniProt: the universal protein knowledgebase in 2023. Nucleic Acids Res. 2023;51(D1):D523–31.
31. Piñero J, Ramírez-Anguita JM, Saüch-Pitarch J, Ronzano F, Centeno E, Sanz F, Furlong LI. The disgenet knowledge platform for disease genomics: 2019 update. Nucleic Acids Res. 2020;48(D1):D845–55.
32. Rappaport N, Nativ N, Stelzer G, Twik M, Guan-Golan Y, Iny Stein T, Bahir I, Belinky F, Morrey CP, Safran M. MalaCards: an integrated compendium for diseases and their annotation. Database. 2013;2013.
33. Amberger JS, Bocchini CA, Schiettecatte F, Scott AF, Hamosh A. OMIM.org: online Mendelian inheritance in man (OMIM®), an online catalog of human genes and genetic disorders. Nucleic Acids Res. 2015;43(D1):D789–98.
34. Szklarczyk D, Kirsch R, Koutrouli M, Nastou K, Mehryary F, Hachilif R, Gable AL, Fang T, Doncheva NT, Pyysalo S. The STRING database in 2023: protein–protein association networks and functional enrichment analyses for any sequenced genome of interest. Nucleic Acids Res. 2023;51(D1):D638–46.
35. Shannon P, Markiel A, Ozier O, Baliga NS, Wang JT, Ramage D, Amin N, Schwikowski B, Ideker T. Cytoscape: a software environment for integrated models of biomolecular interaction networks. Genome Res. 2003;13(11):2498–504.
36. Ge SX, Jung D, Yao R. ShinyGO: a graphical gene-set enrichment tool for animals and plants. Bioinformatics. 2020;36(8):2628–9.
37. Nahoum V, Roux G, Anton V, Rougé P, Puigserver A, Bischoff H, Henrissat B, Payan F. Crystal structures of human pancreatic α-amylase in complex with carbohydrate and proteinaceous inhibitors. Biochem J. 2000;346(1):201–8.
38. Ren L, Qin X, Cao X, Wang L, Bai F, Bai G, Shen Y. Structural insight into substrate specificity of human intestinal maltase-glucoamylase. Protein Cell. 2011;2:827–36.
39. Berger JP, SinhaRoy R, Pocai A, Kelly TM, Scapin G, Gao YD, Pryor KAD, Wu JK, Eiermann GJ, Xu SS. A comparative study of the binding properties, dipeptidyl peptidase-4 (DPP-4) inhibitory activity and glucose-lowering efficacy of DPP-4 inhibitors alogliptin, linagliptin, saxagliptin, sitagliptin, and vildagliptin in mice. Endocrinol Diabetes Metabolism. 2018;1(1):e00002.
40. Morris GM, Huey R, Lindstrom W, Sanner MF, Belew RK, Goodsell DS, Olson AJ. AutoDock4 and AutoDockTools4: automated Docking with selective receptor flexibility. J Comput Chem. 2009;30(16):2785–91.
41. O'Boyle N, Banck M, James CA, Morley C, Vandermeersch T, Hutchison GR. Open babel: an open chemical toolbox. J Cheminform. 2011;3(1):33.
42. Trott O, Olson AJ. AutoDock vina: improving the speed and accuracy of Docking with a new scoring function, efficient optimization, and multithreading. J Comput Chem. 2010;31(2):455–61.
43. Abraham MJ, Murtola T, Schulz R, Páll S, Smith JC, Hess B, Lindahl E. GROMACS: High-performance molecular simulations through multilevel parallelism from laptops to supercomputers. SoftwareX. 2015;1:19–25.
44. Bekker H, Berendsen H, Dijkstra E, Achterop S, Vondrumen R, Vanderspoel D, Sijbers A, Keegstra H, Renardus M. GROMACS—a parallel computer for molecular-dynamics simulations. 4th International Conference on Computational Physics (PC 92).
45. Oostenbrink C, Villa A, Mark AE, Van Gunsteren WF. A biomolecular force field based on the free enthalpy of hydration and solvation: the GROMOS force-field parameter sets 53A5 and 53A6. J Comput Chem. 2004;25(13):1656–76.
46. Lee J, Cheng X, Swails JM, Yeom MS, Eastman PK, Lemkul JA, Wei S, Buckner J, Jeong JC, Qi Y. CHARMM-GUI input generator for NAMD, GROMACS, AMBER, openmm, and charmm/openmm simulations using the CHARMM36 additive force field. J Chem Theory Comput. 2016;12(1):405–13.
47. Lee J, Hitzenberger M, Rieger M, Kern NR, Zacharias M, Im W. CHARMM-GUI supports the amber force fields. J Chem Phys. 2020;153(3):035103.
48. Ogunyemi OM, Gyebi GA, Ibrahim IM, Esan AM, Olaiya CO, Soliman MM, Batiha GE-S. Identification of promising multitargeting inhibitors of obesity from Vernonia amygdalina through computational analysis. Mol Diversity. 2023;27(1):1–25.
49. Ogunyemi OM, Gyebi GA, Ibrahim IM, Olaiya CO, Ocheje JO, Fabusiwa MM, Adebayo JO. Dietary stigmastane-type saponins as promising dual-target directed inhibitors of SARS-CoV-2 proteases: a structure-based screening. RSC Adv. 2021;11(53):33380–98.
50. Gyebi GA, Ogunyemi OM, Ibrahim IM, Afolabi SO, Adebayo JO. Dual targeting of the cytokine storm and viral replication in COVID-19 via plant-derived steroidal pregnanes: an in Silico perspective. Comput Biol Med. 2021;134:104406.
51. Miller IIIBR, McGee TD Jr, Swails JM, Homeyer N, Gohlke H, Roitberg AE. MMPBSA.py: an efficient program for end-state free energy calculations. J Chem Theory Comput. 2012;8(9):3314–21.
52. Valdés-Tresanco MS, Valdés-Tresanco ME, Valiente PA, Moreno E. gmx_MMPBSA: a new tool to perform end-state free energy calculations with GROMACS. J Chem Theory Comput. 2021;17(10):6281–91.
53. Mishra AK, Pandey M, Pannu A, Dewangan HK, Sahoo PK. Review on diabetes mellitus: an insight into the current scenarios, the challenges of therapy, and application of traditional drugs. Curr Traditional Med. 2024;10(3):107–28.
54. Balkrishna A, Sharma N, Srivastava D, Kukreti A, Srivastava S, Arya V. Exploring the safety, efficacy, and bioactivity of herbal medicines: bridging traditional wisdom and modern science in healthcare. Future Integr Med. 2024;3(1):35–49.
55. Wang X, Li J, Shang J, Bai J, Wu K, Liu J, Yang Z, Ou H, Shao L. Metabolites extracted from microorganisms as potential inhibitors of glycosidases (α-glucosidase and α-amylase): A review. Front Microbiol. 2022;13:1050869.
56. Ojo OA, Grant S, Amanze JC, Oni AI, Ojo AB, Elebiyo TC, Obafemi TO, Ayokunle DI, Ogunlakin AD. Annona muricata L. peel extract inhibits carbohydrate metabolizing enzymes and reduces pancreatic β-cells, inflammation, and apoptosis via upregulation of PI3K/AKT genes. PLoS ONE. 2022;17(10):e0276984.
57. Kashtoh H, Baek KH. Recent updates on phytoconstituent alpha-glucosidase inhibitors: an approach toward the treatment of type two diabetes. Plants. 2022;11(20):2722.
58. Mahankali S, Kalava J, Garapati Y, Domathoti B, Maddumala VR, Sundramurty VP. A treatment to cure diabetes using plant-based drug discovery. Evidence-Based Complement Altern Med. 2022;2022:8621665.
59. García-Pérez P, Zhang L, Miras-Moreno B, Lozano-Milo E, Landin M, Lucini L, Gallego PP. The combination of untargeted metabolomics and machine learning predicts the biosynthesis of phenolic compounds in Bryophyllum medicinal plants (Genus Kalanchoe). Plants. 2021;10(11):2430.
60. Pashazadeh H, Redha AA, Koca I. Effect of convective drying on phenolic acid, flavonoid and anthocyanin content, texture, and microstructure of black rosehip fruit. J Food Compos Anal. 2024;125:105738.
61. Paul A, Acharya K, Chakraborty N. Involvement of phenylpropanoid pathway and Shikimic acid pathway in environmental stress response. Biology and biotechnology of environmental stress tolerance in plants. Apple Academic. 2023. pp. 27–66.
62. Tak Y, Kaur M, Gautam C, Kumar R, Tilgam J, Natta S. Phenolic biosynthesis and metabolic pathways to alleviate stresses in plants. Plant phenolics in abiotic stress management. Springer Nature Singapore. 2023:63–87.
63. Haldar S, Lee SH, Tan JJ, Chia SC, Henry CJ, Chan EC. Dose-dependent increase in unconjugated cinnamic acid concentration in plasma following acute consumption of polyphenol-rich curry in the polyspice study. Nutrients. 2018;10(7):934.
64. Mueed A, Ibrahim M, Shibli S, Madjirebaye P, Deng Z, Jahangir M. The fate of flaxseed-lignans after oral administration: A comprehensive review on its bioavailability, pharmacokinetics, and food design strategies for optimal application. Crit Rev Food Sci Nutr. 2024;64(13):4312–30.
65. Fernández-Ochoa Á, Cádiz-Gurrea MD, Fernández-Moreno P, Rojas-García A, Arráez-Román D, Segura-Carretero A. Recent analytical approaches for the study of bioavailability and metabolism of bioactive phenolic compounds. Molecules. 2022;27(3):777.
66. Tomas M, Wen Y, Liao W, Zhang L, Zhao C, McClements DJ, Nemli E, Bener M, Apak R, Capanoglu E. Recent progress in promoting the bioavailability of polyphenols in plant-based foods. Crit Rev Food Sci Nutr. 2024:1–22.
67. Shimsa S, Soumya NP, Mondal S, Mini S. Syringic acid affords antioxidant protection in the pancreas of type 2 diabetic rats. Bioactive Compd Health Disease. 2023;6(2):13–25.
68. Adisakwattana S. Cinnamic acid and its derivatives: mechanisms for prevention and management of diabetes and its complications. Nutrients. 2017;9(2):163.
69. Parveen S, Shehzadi S, Shafiq N, Rashid M, Naz S, Mehmood T, Riaz R, Almaary KS, Nafidi HA, Bourhia M. A discovery of potent Kaempferol derivatives as multitarget medicines against diabetes as well as bacterial infections: an in Silico approach. J Biomol Struct Dynamics. 2024:1–23.
70. Yu M, Zhu S, Huang D, Tao X, Li Y. Inhibition of starch digestion by phenolic acids with a cinnamic acid backbone: structural requirements for the Inhibition of α-amylase and α-glucosidase. Food Chem. 2024;435:137499.
71. Chandarajoti K, Kara J, Suwanhom P, Nualnoi T, Puripattanavong J, Lee VS, Tipmanee V, Lomlim L. Synthesis and evaluation of coumarin derivatives on

antioxidative, tyrosinase inhibitory activities, melanogenesis, and in Silico investigations. Sci Rep. 2024;14(1):5535.
72. El-Askary H, Salem HH, Abdel Motaal A. Potential mechanisms involved in the protective effect of Dicaffeoylquinic acids from Artemisia annua L. leaves against diabetes and its complications. Molecules. 2022;27(3):857.
73. Bouslamti M, Loukili EH, Elrherabi A, El Moussaoui A, Chebaibi M, Bencheikh N, Nafidi HA, Bin Jardan YA, Bourhia M, Bnouham M, Lyoussi B. Phenolic profile, Inhibition of α-amylase and α-glucosidase enzymes, and antioxidant properties of Solanum elaeagnifolium cav. (Solanaceae): in vitro and in Silico investigations. Processes. 2023;11(5):1384.
74. Fan J, Johnson MH, Lila MA, Yousef G, De Mejia EG. Berry and citrus phenolic compounds inhibit dipeptidyl peptidase IV: implications in diabetes management. Evidence-Based Complementary and Alternative Medicine. 2013;2013.
75. Jia Y, Cai S, Muhoza B, Qi B, Li Y. Advance in dietary polyphenols as dipeptidyl peptidase-IV inhibitors to alleviate type 2 diabetes mellitus: aspects from structure-activity relationship and characterization methods. Crit Rev Food Sci Nutr. 2023;63(19):3452–67.
76. Ruwizhi N, Aderibigbe BA. Cinnamic acid derivatives and their biological efficacy. Int J Mol Sci. 2020;21(16):5712.
77. Thorat SU, Jain RK, Ramalingam K, Ali S, Ganesh S. Evaluation of cytotoxicity of 4-hydroxycinnamic acid using tetrazolium bromide assay and zebrafish embryotoxicity: an in vitro study. Cureus. 2024;16(3).
78. Ogunlakin AD, Sonibare MA, Yeye OE, Jabeen A, Shah SF, Ojo OA, Gyebi GA, Ayokunle DI. Design, synthesis, and characterization of cinnamic acid derivatives with two novel acrylohydrazones on HeLa and CHO-1 cancer cell lines: the experimental and computational perspective. Chem Afr. 2024;7(2):583–604.
79. Marangi F, Pinto D, de Francisco L, Alves RC, Puga H, Sut S, Dall'Acqua S, Rodrigues F, Oliveira MB. Hardy Kiwi leaves extracted by multifrequency multimode modulated technology: A sustainable and promising byproduct for industry. Food Res Int. 2018;112:184–91.
80. Peperidou A, Kapoukranidou D, Kontogiorgis C, Hadjipavlou-Litina D. Multitarget molecular hybrids of cinnamic acids. Molecules. 2014;19(12):20197–226.
81. Mielecki M, Lesyng B. Cinnamic acid derivatives as inhibitors of oncogenic protein kinases–structure, mechanisms and biomedical effects. Curr Med Chem. 2016;23(10):954–82.
82. Martiz RM, Patil SM, Abdulaziz M, Babalghith A, Al-Areefi M, Al-Ghorbani M, Mallappa Kumar J, Prasad A, Mysore Nagalingaswamy NP, Ramu R. Defining the role of isoeugenol from Ocimum tenuiflorum against diabetes mellitus-linked alzheimer's disease through network Pharmacology and computational methods. Molecules. 2022;27(8):2398.
83. Jiao X, Jin X, Ma Y, Yang Y, Li J, Liang L, Liu R, Li Z. A comprehensive application: molecular Docking and network Pharmacology for the prediction of bioactive constituents and Elucidation of mechanisms of action in component-based Chinese medicine. Comput Biol Chem. 2021;90:107402.
84. Li X, Xia Y-L, Ai S-M, Liang J, Sang P, Ji X-L, Liu S-Q. Insights into protein–ligand interactions: mechanisms, models, and methods. Int J Mol Sci. 2016;17(2):144.
85. Marushchak M, Krynytska I. Does TP53 gene polymorphism increase the risk of obesity and chronic pancreatitis comorbidities in type 2 diabetic patients? Romanian J Diabetes Nutr Metabolic Dis. 2022;29(1):96–103.
86. Kochetova OV, Shangareeva ZA, Avsaleydiniva DS, Viktorova TV, Korytina GF. The role of the AKT1 gene in the pathogenesis of type 2 diabetes mellitus and its complications. Molekulyarnaya Meditsina (Molecular Medicine). 2024;22(3):57–64.
87. Rezaeepoor M, Hoseini-Aghdam M, Sheikh V, Eftekharian MM, Behzad M. Evaluation of interleukin-23 and JAKs/STATs/SOCSs/ROR-γt expression in type 2 diabetes mellitus patients treated with or without sitagliptin. J Interferon Cytokine Res. 2020;40(11):515–23.
88. Pickup JC, Chusney GD, Thomas SM, Burt D. Plasma interleukin-6, tumor necrosis factor α and blood cytokine production in type 2 diabetes. Life Sci. 2000;67(3):291–300.
89. Murakoshi M, Gohda T, Suzuki Y. Circulating tumor necrosis factor receptors: a potential biomarker for the progression of diabetic kidney disease. Int J Mol Sci. 2020;21(6):1957.
90. Zhang W, Thompson BJ, Hietakangas V, Cohen SM. MAPK/ERK signaling regulates insulin sensitivity to control glucose metabolism in Drosophila. PLoS Genet. 2011;7(12):e1002429.
91. Yan Z, Cao X, Sun S, Sun B, Gao J. Inhibition of GSK3B phosphorylation improves glucose and lipid metabolism disorder. Biochim Et Biophys Acta: Mol Basis Disease. 2023;1869(6):166726.
92. Wang ZY, Guo MQ, Cui QK, Yuan H, Fu SJ, Liu B, Xie F, Qiao W, Cheng J, Wang Y. PARP1 deficiency protects against hyperglycemia-induced neointimal hyperplasia by upregulating TFPI2 activity in diabetic mice. Redox Biol. 2021;46:102084.
93. Calabrese V, Cornelius C, Leso V, Trovato-Salinaro A, Ventimiglia B, Cavallaro M, Scuto M, Rizza S, Zanoli L, Neri S. Oxidative stress, glutathione status, Sirtuin and cellular stress response in type 2 diabetes. Biochim Et Biophys Acta: Mol Basis Disease. 2012;1822(5):729–36.
94. Zavodnik I, Dremza I, Lapshina E, Cheshchevik V. Diabetes mellitus: metabolic effects and oxidative stress. Biochem (Moscow) Supplement Ser A: Membr Cell Biology. 2011;5:101–10.
95. Onyango AN. Cellular stresses and stress responses in the pathogenesis of insulin resistance. Oxidative Med Cell Longev. 2018;2018:4321714.
96. Gannon MC, Nuttall FQ, Saeed A, Jordan K, Hoover H. An increase in dietary protein improves the blood glucose response in persons with type 2 diabetes. Am J Clin Nutr. 2003;78(4):734–41.
97. Fraenkel M, Ketzinel-Gilad M, Ariav Y, Pappo O, Karaca M, Castel J, Berthault MF, Magnan C, Cerasi E, Kaiser N. mTOR Inhibition by Rapamycin prevents β-cell adaptation to hyperglycemia and exacerbates the metabolic state in type 2 diabetes. Diabetes. 2008;57(4):945–57.
98. Nagaraj V, Kazim AS, Helgeson J, Lewold C, Barik S, Buda P, Reinbothe TM, Wennmalm S, Zhang E, Renström E. Elevated basal insulin secretion in type 2 diabetes caused by reduced plasma membrane cholesterol. Mol Endocrinol. 2016;30(10):1059–69.
99. Huang X, Liu G, Guo J, Su Z. The PI3K/AKT pathway in obesity and type 2 diabetes. Int J Biol Sci. 2018;14(11):1483.
100. Rao SN, Head MS, Kulkarni A, LaLonde JM. Validation studies of the site-directed Docking program LibDock. J Chem Inf Model. 2007;47(6):2159–71.
101. Li Y, Zheng X, Yi X, Liu C, Kong D, Zhang J, Gong M. Myricetin: a potent approach for the treatment of type 2 diabetes as a natural class B GPCR agonist. FASEB J. 2017;31(6):2603.
102. Niisato N, Marunaka Y. Therapeutic potential of multifunctional myricetin for treatment of type 2 diabetes mellitus. Front Nutr. 2023;10:1175660.
103. Azam SS, Abbasi SW. Molecular Docking studies for the identification of novel melatoninergic inhibitors for acetylserotonin-O-methyltransferase using different Docking routines. Theoretical Biology Med Model. 2013;10:1–16.
104. Habtemariam S, Lentini G. The therapeutic potential of Rutin for diabetes: an update. Mini-Reviews Med Chem. 2015;15(7):524–8.
105. Ali M, Hassan M, Ansari SA, Alkahtani HM, Al-Rasheed LS, Ansari SA. Quercetrin and Kaempferol as multitargeting antidiabetic agents against mouse model of chemically induced type 2 diabetes. Pharmaceuticals. 2024;17(6):757.
106. Huang PK, Lin SR, Chang CH, Tsai MJ, Lee DN, Weng CF. Natural phenolic compounds potentiate hypoglycemia via Inhibition of dipeptidyl peptidase IV. Sci Rep. 2019;9(1):15585.
107. Gyebi GA, Ogunyemi OM, Adefolalu AA, Rodríguez-Martínez A, López-Pastor JF, Banegas-Luna AJ, Pérez-Sánchez H, Adegunloye AP, Ogunro OB, Afolabi SO. African derived phytocompounds May interfere with SARS-CoV-2 RNA capping machinery via Inhibition of 2'-O-ribose methyltransferase: an in Silico perspective. J Mol Struct. 2022;1262:133019.
108. Chiang YC, Wong MT, Essex JW. Molecular dynamics simulations of antibiotic Ceftaroline at the allosteric site of penicillin-binding protein 2a (PBP2a). Isr J Chem. 2020;60(7):754–63.
109. Leimkuhler B, Matthews C. Molecular dynamics. Interdisciplinary Appl Math. 2015;39(1).
110. Kollman PA, Massova I, Reyes C, Kuhn B, Huo S, Chong L, Lee M, Lee T, Duan Y, Wang W. Calculating structures and free energies of complex molecules: combining molecular mechanics and continuum models. Acc Chem Res. 2000;33(12):889–97.

Publisher's note

Springer Nature remains neutral with regard to jurisdictional claims in published maps and institutional affiliations.